A MODEL FOR THE TIME DEPENDENT BEHAVIOUR OF ROCK JOINTS

by

NICHOLAS JULIAN CAMP
BSc (Eng) Civil, University of Cape Town

A thesis submitted in partial fullfilment of the requirements for the degree of Master of Science in Engineering.

Department of Civil Engineering
University of Cape Town

September 1989

To Francesca, for her unflagging support, help and patience throught my MSc.

DECLARATION OF CANDIDATE

I, Nicholas Julian Camp, declare that this thesis is my own work and that it has not been submitted for a degree at another university.

N J CAMP

SEPTEMBER 1989

SYNOPSIS

This thesis is a theoretical investigation into the time-dependent behaviour of rock joints. Much of the research work that has been conducted to date in the area of finite element analysis has been involved with the development of special elements to deal with these discontinuities. A comprehensive literature survey is undertaken highlighting some of the significant contributions to the modelling of joints.

It is then shown how internal variables can be used to model discontinuities in the rock mass. A finite element formulation is described resulting in a system of equations which can easily be adapted to cope with various constitutive behaviours on the discontinuities. In particular, a viscoplastic relationship, which uses a homogeneous, hyperbolic yield function is adopted. The viscoplastic relationship can be used for both time-dependent (creep) or quasi-static (elasto-plastic) problems.

Time-dependent behaviour requires a time integration scheme and therefore a generalised explicit/implicit scheme is chosen. The resulting numerical algorithms are all implemented in the finite element program, NOSTRUM.

Various examples are presented to illustrate certain features of both the formulation and the numerical algorithm. Jointed rock beams and a jointed infinite rock mass are modelled assuming plane strain conditions. Reasons are proposed to explain the predicted behaviour.

The results of the analysis shows that the internal variable formulation successfully models time-dependent joint movements in a continuous media. The method gives good, qualitative results which agree with observations in deep level mines.

It is recommended that quantitative mine observations be used to calibrate the model so that usable predictions of joint movement can be made. This would enable any new developments to be implemented in the model. Further work on implicit methods might allow greater modelling flexibility by reducing computer run times.

ACKNOWLEDGEMENTS

The author wishes to thank the following :

Dr W W Bird, Department of Civil Engineering, U C T for his help and insight during the past year.

Prof J B Martin, Dean of Engineering, U C T for his encouragement and guidance.

The Chamber of Mines Research Organisation, for their financial assistance.

Cheryl Wright, for typing my thesis so splendidly.

TABLE OF CONTENTS

LIST OF FIGURES

NOMENCLATURE

		Dimensions
A	parameter defining turning point of hyperbola	N
a	c/T	N
c	cohesion	N
$\underline{D}$	elastic property matrix	N/m^2
E	Young's modulus	N/m^2
G^e	elastic shear modulus	N/m^2
$\underline{H}$	element stiffness submatrix	-
i	dilation angle	degrees
i_o	initial dilation angle	degrees
J^e	elemental strain energy	-
JCS	joint wall compressive strength	N/m^2
JRC	joint roughness coefficient	-
$\underline{K}$	standard elastic element stiffness matrix	-
K^e	elastic bulk modulus	N/m^2
$\underline{k}$	material property matrix	-
k_e	joint circumferential stretching stiffness	-
k_n	joint normal stiffness	-
k_w	joint rotation stiffness	-
k_r	joint radial stretching stiffness	-
k_s	joint shear stiffness	-
k_{sn}, k_{ns}	joint cross stiffnesses	-
L	length of the joint	m
$\underline{L}$	element stiffness submatrix	-
M_o	bending moment	Nm
$\underset{\sim}{m}$, $\underset{\sim}{n}$	shear and normal vectors which define slip surface	-
$\underset{\sim}{P}$	applied force vector	N
$2q$	maximum deviator stress	N/m^2
$\underset{\sim}{R}$	nodal force vector	N
T	tan θ	degrees
t	element thickness	m
Δt_c	critical time step length	hr

$\underset{\sim}{u}$	displacement vector	m
$\underset{\sim}{u}^+$, $\underset{\sim}{u}^-$	nodal displacement on positive or negative side of the slip line	m
Δu	change in horizontal displacement	m
Δv	change in vertical displacement	m
$\underset{\sim}{X}$	internal nodal force vector	N
β	integration factor	-
ϵ_n	normal strain	-
ϵ_s	shear strain	-
ϵ_{shear}	maximum deviatoric strain	-
ϵ_{vol}	volumetric strain	-
θ	angle of internal friction for the joint	degrees
λ_n	normal joint dislocation	m
λ_s	shear joint dislocation	m
$\dot{\underset{\sim}{\lambda}}$	dislocation rate w.r.t. time i.e. $\frac{\partial \underset{\sim}{\lambda}}{\partial t}$	m/sec
σ_n	normal stress	N/m^2
$\Delta\sigma_n$	change in normal stress	N/m^2
σ_{oct}	octahedral normal stress	N/m^2
τ	shear stress	N/m^2
ν	Poisson's Ratio	-
ϕ_b	friction angle for a smooth surface	degrees
ϕ_p	peak friction angle	degrees
ϕ_r	residual friction angle	degrees
$\Delta\omega$	change in relative rotation of joint surfaces	rads

CHAPTER 1

INTRODUCTION

Every year mining operations take place at greater and greater depths. At present mining is conducted at depths greater than 3 600 m below the surface and even the most rudimentary calculations show that the strength of the rock is easily exceeded. The high stresses at this depth result in extensive fracturing of the rock mass particularly around the mined out area of the stope. The stope occurs in stratified rock with bedding or parting planes at approximately 1 m intervals. The lack of cohesion in the parting planes suggests that separation will occur along the parting planes and that each layer will support its own weight. The layer immediately above the stope is known as the hanging wall beam.

The hanging wall beam is traversed by a number of shear fractures. These shear fractures originate between 6 m and 8 m ahead of the advancing stope and separate the rock into relatively intact material. The shear fractures have negligible cohesion and contain a powdery white material. It is along these fractures that the majority of shear movement takes place.

Time-dependent movement of the rock mass has been observed as a result of the relaxation of the stresses in the rock. It is known that creep takes place in the rock mass as well as along the joints but the overall response of the rock mass is dominated by movements on the joints or parting planes. Therefore this study focuses only on the time-dependent behaviour of the rock joints.

The aim of this thesis is to develop an alternative to the special joint or interface elements normally used to model discontinuities and joints. A further aim is to deal with time-dependent movement along the discontinuities. The internal variable formulation combined with finite element approximations is used to model this behaviour. A viscoplastic constitutive law and a general time integration scheme is implemented.

The scope of this study is to :

1. Implement a viscoplastic constitutive law with a hyperbolic yield function.

2. Develop an explicit/implicit computer program to model joint movements.

3. Show that the development of dislocations and their associated forces on the discontinuities are time-dependent.

4. Offer some explanations for the similarities between the observed behaviour and the numerical results.

In Chapter 2 a comprehensive literature survey is presented which highlights some of the important developments in theoretical and empirical joint models proposed from 1966 to the present.

In Chapter 3 the internal variable formulation is presented. The various terms, vectors and matrices used in the formulation are defined. The ease with which finite element approximations can be adopted is shown. The stiffness matrix assembly process is discussed.

The theory of viscoplastic behaviour is covered in Chapter 4. The flow equation and the form in which it is used is presented. The formulation of the hyperbolic yield function is discussed in detail.

The various explicit and implicit time integration schemes are covered in Chapter 5. Criteria for evaluating critical time step lengths are briefly discussed.

Finally, in Chapter 6, various examples are presented which illustrate important characteristics of the model. A hanging wall beam with an increasing number of vertical joints is studied. The compressive axial force and the relationship between shear and normal dislocations are studied. A further example of a joint in an infinite rock mass is also presented.

These examples show that in the absence of reliable observed data from an actual mining situation, the program gives good qualitative results for a number of mining problems. The program provides insight into the essential features of the problem rather than providing specific numerical results for particular cases.

CHAPTER 2

LITERATURE SURVEY

2.1 INTRODUCTION

The decisive role of joints, faults and discontinuities in rock mass behaviour have been known to engineers and geologists for a long time. Most rock failures occur on joints or discontinuities which separate large masses of intact rock. Not only is the movement in the rock mass dominated by movement on the joints but there is also a pronounced reduction in the global deformation modulus and the strength of the rock. Joints may occur in "families" where their size and spacing also has a marked effect on any deformations that take place.

In the past, a great deal of attention has been paid to mathematical models which describe the behaviour of intact rock. Although these models may describe elastic and visco-elastic behaviour very closely, no continuum model, by itself, can predict the behaviour of a rock mass with discontinuities or joints.

Some attempts have been made to take joints into account when modelling underground problems. Three different approaches have generally been adopted.

In the first approach, joints are modelled using discrete interface elements in either two or three dimensions. These have the drawback of numerical ill-conditioning caused by very large off diagonal terms in the stiffness matrix. To a certain extent these problems have been overcome by using the relative displacement of the two sides of the element as an independent degree of freedom and by the development of eight-noded isoparametric elements.

The second approach alters the constitutive laws and material parameters of the intact rock to take account of joints. The rock joints are then assumed to be ubiquitous. This approach is used when the characteristic size of joints is small and they are evenly distributed throughout the rock mass. The rock mass is then still treated as a continuum.

The final approach is that of the mechanics of discontinua or clastic mechanics where the rock mass is modelled as an assemblage of blocks or discs. The contacts between adjacent blocks are modelled using linear or non-linear rheological elements. The history of deformations can be found by successive applications of the equilibrium equations and the stress-strain laws. This is the approach adopted by Belytschko *et al* [1].

Other researchers performed experiments on various rock types and artifically made joints and attempted to predict joint behaviour. Patton [2], Krahn and Morgenstern [3], Reeves [4] and Dight and Chiu [5] examined the surface roughness of joints and correlated this to the frictional strength of the joint and the shear and normal behaviour of the joint. Bandis *et al* [6] conducted studies on scale effects of the shear behaviour of rock joints and found that the peak shear strength and shearing characteristics were strongly scale dependent.

2.2 GENERAL CHARACTERISTICS OF JOINTS

Although there are many types of joints, there are certain characteristics which apply to all joints. These characteristics are listed below :

(a) Joints more closely resemble irregular lines than zones of appreciable thickness.

(b) The resistance to a net normal tensile force is negligible.

(c) There is a high resistance to a net normal compressive force. Compressive deformation can take place if crushing of asperities occurs.

(d) As the normal compressive stress on the joint increases there is less tendency for the joint to dilate when sheared.

(e) In its simplest form, the shear strength may be represented by a linear Mohr envelope.

(f) As the shear stress increases, small elastic deformations will occur before the yield stress is reached.

Depending on the type of joint, the relative importance of each of the above criteria will vary, but these are essentially characteristics common to all joint surfaces. Joints also exhibit certain characteristic behaviour patterns. If a shear stress is applied along the joint there is an associated dilation or normal displacement across the joint.

Four different stages of joint behaviour have been summarised by Roberds and Einstein [7]. When shearing occurs at low normal stresses, the rock faces forming either side of the discontinuity slide over one another without shearing off any asperities. As the normal stress increases, the dominant asperities are sheared through while others are overridden. If the normal stress remains constant the large remaining asperities will slide over one another as shearing along the joint continues. As the normal stresses increase still further, all the asperities are sheared off at relatively small shear strains and strain-softening behaviour occurs. Finally, the stresses are so high that there is a transition from shearing through the asperities to fracturing through the intact rock. Here strain-hardening of the intact rock occurs.

Dilatancy is a very important characteristic of joint behaviour. Sofianos [8] found that joint dilation occurring in the roof blocks of a tunnel or stope cause an increase in the normal stress which exerts a stabilising influence. Dilatancy must not be confused with Poisson's effect. Poisson's ratio, ν , relates normal strains in one direction to normal strains in another. Dilatancy relates normal strains and shear strains. Whereas a tension specimen pulls inwards and a compression specimen bulges outwards when loaded, most rock fractures will be dilatant regardless of the direction of applied shear. The importance of this distinction is that the stability of a large joint block is improved by a large dilatancy value whereas it is worsened by a large value of Poisson's ratio. From this it follows that a dilatant joint which is tested in direct shear but constrained to have a constant normal displacement would have a higher frictional strength than when tested under constant normal stress.

The amount a rock joint will dilate is governed by the roughness of the rock surfaces and the infilling material. The roughness is generally caused either by sedimentary or metamorphic processes. The behaviour of joints that are open or filled would be contractant whereas closed or healed joints would be dilatant. Goodman and Dubois [9] have attempted to classify types of joints with respect to dilatancy and coupled shear displacement.

Various researchers have developed relationships between the shear and normal stresses and the resulting shear and normal displacements on the joint surface. These relationships, which take the form of constants, are obtained from direct shear and normal tests on joint surfaces. These constants are called the unit joint stiffnesses. If a rock joint of length L and unit width is subjected to direct shear with an applied normal force after initial elastic deformation has occurred, the asperities in the joint deform. By subtracting the elastic deformation from the total deformation the joint normal deformation W_n can be found. This can then be plotted against the applied force per unit length and a typical result is shown in Figure 2.1.

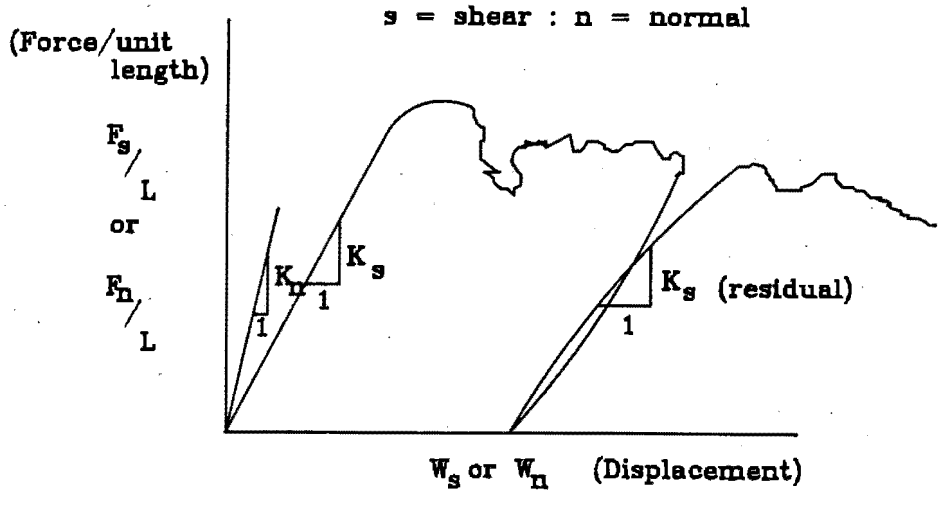

Evaluation of shear or normal unit joint stiffnesses from direct testing.

FIG 2-1

The same procedure is used to obtain the shear unit joint stiffness. The unit joint stiffness terms are given by k_n and k_s and together form the material property matrix :

$$\underline{k} = \begin{bmatrix} k_s & 0 \\ 0 & k_n \end{bmatrix} \qquad (2.1)$$

The off diagonal terms or joint cross stiffnesses are set equal to zero. This means that the stiffness of the material transverse to the direction of shear is ignored. This approach cannot be correct because the normal stress increase due to shear displacement definitely depends on the stiffness of the material adjacent to the joint. Although the above relationships are precise when there is no dilatancy they are ambiguous when there is coupled shear and normal displacement and it is then no longer reasonable to set the off diagonal terms to zero. In only one paper, that of Goodman and Dubois [9], were any values for the cross stiffnesses found.

Heuze and Barbour [10] believe that in order to simulate representative dilatant joint behaviour in a test rig, the shear test system should have the same transverse stiffness as the stiffness of the adjacent rock in the field. They believe that to obtain representative dilatant joint effects the transverse stiffness of each joint to be modelled would have to be determined in the field. This seems to be an unnecessary requirement because it implies that values of k_n and k_s would also have to be obtained for each joint. It seems far more reasonable to obtain representative values of the joint stiffness and use them with a safety factor or use a "worst case" combination of the three stiffness terms.

Another joint parameter defined by Goodman *et al* [11] is the shear strength, S along the joint which can be described by c and ϕ, the cohesion and internal angle of friction respectively. The joint stiffnesses and the shear strength can characterise a joint and serve as a base to predict the behaviour of a joint under load. The most

important factors influencing the joint parameters are the contact area ratio between the two joint walls, the perpendicular aperture distribution and amplitude, the roughness of the walls, the friction along the joint, the cohesion due to interlocking and any relevant properties of the infilling material if present. The type of filling material can have a large effect on the joint parameters. Clay minerals such as montmorillonite are extremely slippery when wet and have negligible shear strength. Joints filled with quartz or calcite can give properties that are as good or sometimes better than the rock wall properties. These joints can be viewed as being inherently stable. If there is enough ground water, a mineral such as calcite may dissolve over time causing the joint to become unstable again.

Goodman [12] demonstrated that when the thickness of the infilling material was more than twice the height of the asperities, the strength and deformation characteristics of the joint could be taken as the same as those of the infilling material. This reduces the aspect ratio of the joint but makes it more of a two-dimensional problem than a one-dimensional problem. The joints can still be successfully modelled using interface elements which can be either 4 or 8-noded isoparametric elements.

2.3 HISTORY OF DEVELOPMENT OF JOINT MODELS

Patton 1966 [2] performed some direct shear test on plaster of paris specimens which had been cast with irregular surfaces. The asperity angles moulded into the specimens varied between 25° and 55°. Patton found that the coefficient of friction for a natural rough joint surface could be expressed as the sum of the sliding friction angle ϕ_b, and the angle of inclination of the asperities $\pm i$. The sign of i indicates whether contraction or dilation on the joint takes place. The

yield criterion is a bilinear Mohr envelope given by

$$\tau = \bar{\sigma}_n \tan (\phi_b + i) \quad \text{for} \quad \bar{\sigma}_n < \bar{\sigma}_n^* \tag{2.2}$$

$$\tau = C + \bar{\sigma} \tan \phi_r \quad \text{for} \quad \bar{\sigma}_n > \bar{\sigma}_n^* \tag{2.3}$$

where $\bar{\sigma}_n^*$ = yield stress of the intact rock

ϕ_b = initial friction angle for smooth surface

ϕ_r = residual friction angle

C = cohesion.

This is a plasticity model because the post yield behaviour at any normal stress gives zero normal strain with unlimited shear strain. The flow rule is derived from the geometry of the discontinuity surface i.e. $(-\delta \epsilon_{norm} / \delta \epsilon_{shear}) = \tan i$ and it is assumed that there are no post-yield elastic strains.

The drawbacks of this model are the assumption of a single asperity angle and the assumption that only post yield strain ratios and not strains are described. There are also numerical difficulties caused by the kink in the yield surface at $\bar{\sigma}_n = \bar{\sigma}_n^*$.

The first attempt to model joints, using specially developed elements suitable for a finite element code, was done by Goodman, Taylor & Brekke (1968) [11]. They developed a four noded element which was compatible with continuum elements and which could be added into the structural stiffness matrix. The concept of relative displacements given by a vector $\underset{\sim}{w}$ was introduced. This displacement vector represents the relative horizontal and vertical movement of the upper and lower sides of the element. The force vector $\underset{\sim}{P}$ may be expressed as a product of

$\underline{k}$, a diagonal material property matrix and the relative displacements $\underset{\sim}{w}$. The matrix $\underline{k}$ is once again given by

$$\underline{k} = \begin{bmatrix} k_s & 0 \\ 0 & k_n \end{bmatrix} \qquad (2.4)$$

where k_s and k_n are the unit joint stiffnesses in the tangential and normal directions respectively. The derivation of these terms was described earlier. Initially, the coordinates of the corresponding corner nodes are the same. This gives the element zero thickness. The displacements of the corner nodes are given by a vector $\underset{\sim}{u}$ and for each node the displacement has a horizontal and a vertical component. The result is an 8 by 8 stiffness matrix which depends solely on two quantities - the tangential and normal unit joint stiffnesses.

For computer implementation the joint cohesion, joint friction and residual tangential stiffness are input as data together with the unit joint stiffnesses. The shear strength is calculated from the normal pressure on each joint. If the joint shear stress exceeds the shear strength, k_s is set equal to $k_{s\ residual}$ and the computation is repeated. If the normal stress on any joint becomes tensile, both k_s and k_n are set equal to zero and the computation is repeated.

This model gives a good account of pre-yield behaviour but strain softening is always assumed. Goodman does not attempt to relate the cross stiffnesses k_{ns} and k_{sn} even though it is clear that the shear and normal stress-strain behaviours are dependent on each other.

This model does not account for unloading or reloading, and furthermore the rotations are not taken into account. Another important factor is that it is a non-dilatant model and the shear and normal deformation can only be related indirectly by relating shear and normal stresses. Difficulties, due to numerical ill-conditioning of the stiffness matrix, may arise. These problems are caused by large off-diagonal terms and small diagonal terms in the stiffness matrix.

Ladanyi and Archambault (1970) [13] proposed an elasto-plastic model which assumes a stress dependent change in the asperity angle i. The initial value is given by i_o which corresponds to the angle of the steepest dominant asperity. As the normal stresses are increased, the asperities are sheared off and i decreases to zero. As the normal stresses are increased still further, the angle i becomes more negative, indicating closing of the joint. This continues until the discontinuity is completely closed and the angle i reaches a value of i_m.

The stress dependency of i is given by

$$i = (i_o - i_m)\left[\frac{\bar{\sigma}_m - \bar{\sigma}_n}{\bar{\sigma}_m}\right]^{k_2} + i_m \qquad (2.5)$$

where $\bar{\sigma}_m$ is the stress at which $i = i_m$

k_2 is an experimentally derived constant and is approximately equal to 4.0.

At low values of $\bar{\sigma}_n$, shearing produces dilatancy but above a value of $\bar{\sigma}_n = \bar{\sigma}_m$, dilatancy will not occur. Ladanyi believes that when $\bar{\sigma}_m$ is reached, the joint is closed along its entire length.

A special case of equation (2.5) occurs when the applied normal stress is just enough to stop dilatancy. This means $i_m = 0$ and $\bar{\sigma}_m = \bar{\sigma}_T$ and equation (2.5) is simplified to

$$i = i_o\left[\frac{\bar{\sigma}_T - \bar{\sigma}_n}{\bar{\sigma}_T}\right]^{k_2} \qquad (2.6)$$

The flow rule in this model is similar to the Patton model and assumes perfectly plastic behaviour after yielding.

At some stress value $\bar{\sigma}_t$, there is a transition of behaviour from shearing taking place through the asperities to shearing through the intact rock. The plastic potential in this case should have a shape which is concave to the $\bar{\sigma}_n$ axis for the intact material. The flow rule for this yield function will then be non-associated.

The limitations of this model are that no preyield behaviour is considered. The assumption of perfectly-plastic post yield behaviour means that strain hardening or softening behaviour cannot be modelled. Both this model and the Patton model are mainly concerned with the behaviour just at yield.

Ghaboussi, Wilson & Isenberg (1973) [14] improved on the element developed by Goodman *et al* by including positive and negative dilatancy. It could be used with axisymmetric or plane continuous finite elements. An important feature of this element was that relative displacements were used as independent degrees of freedom. This results in the displacements on one side of the slip surface being transformed into relative displacements between the two sides of the slip surface. The joint element has four degrees of freedom and the displacements are assumed to vary linearly along the length of the element. The stresses and strains are related by a material property matrix comprised of joint stiffness terms in the normal and shear directions. The material property matrix takes a different form depending on whether dilatant or non-dilatant joints are being modelled. For non-dilatant joints the off diagonal terms are zero because the normal and shear components of deformation are uncoupled. The stress-strain relationship is assumed to be elastic-perfectly plastic using a Mohr-Coulomb yield criteria.

The material property matrix for dilatant joints is considerably more complicated. The orientation of the asperity is related to the orientation of the joint surface using a transformation matrix. The amount of dilatancy depends on the joint stiffness, the geometry of the joint and the normal stress.

Another more advanced model proposed by Ghabousi *et al* is one that does not use critical state concepts like the previous model, but is based on general elasto-plastic concepts. A two part yield surface with an associated flow rule is assumed.

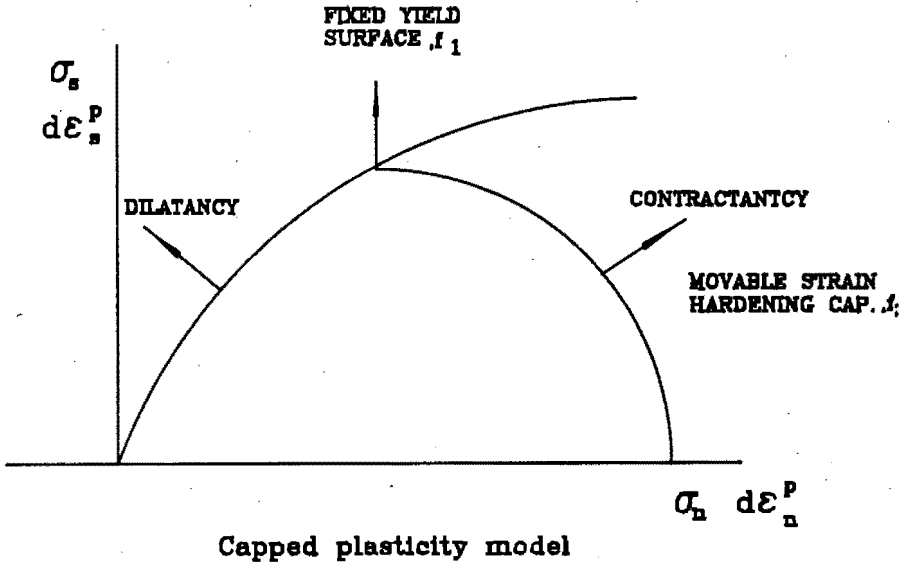

Capped plasticity model

FIG 2-2

This method of representing dilatant behaviour of joints involves the use of the capped plasticity model shown in Figure 2.2. A perfectly plastic yield surface f_1, controls stresses and a strain hardening cap f_2 controls dilatancy. A strain hardening parameter k, may be defined for f_2 so that the cap moves in the compressive σ_n direction while contracting and in the tensile σ_n direction while dilating. Where curves f_1 and f_2 intersect, perfectly plastic shear strain with zero normal strain behaviour occurs.

This model has a number of limitations. Firstly, it will over-estimate dilation by assuming an associated flow rule. Secondly, no strain softening can be modelled. Lastly, the residual shear stress condition for strain hardening behaviour will be over-estimated if it is assumed that the strain hardening behaviour will continue beyond the critical state at constant volume to curve f_1.

In direct contrast to the theoretical model above, Barton (1976) [15] developed an empirical model. The yield criteria for the rock discontinuity is given by

$$\tau = \bar{\sigma}_n \tan \left[\text{JRC} \log \left(\frac{\text{JCS}}{\bar{\sigma}_n}\right) + \phi_b \right] \qquad (2.7)$$

where JRC is a joint roughness coefficient ranging from 0 to 20, JCS is the joint wall compressive stress and ϕ_b is the basic angle of friction of a flat, non-dilatant rock surface. At yield the flow rule is non-associative and the peak dilation rate is determined experimentally as

$$\left(\frac{\delta \epsilon_n}{\delta \epsilon_s}\right) = \tan \left[\frac{\text{JRC}}{2} \log \left(\frac{\text{JCS}}{\bar{\sigma}_n}\right) \right] . \qquad (2.8)$$

At the transition from ductile to brittle failure Barton defines a critical state line inclined at ϕ_c which equals 26.6° for all rocks. It is possible that ϕ_b could be greater or less than ϕ_c. This implies that the rock has reached a critical state before it is close to yielding. Another drawback of the model is that it only describes peak behaviour and not pre or post yield behaviour. It is therefore a time-independent model.

Goodman and St John (1977) [16] have developed a joint element where rotation is explicity considered. The material property matrix relates the stresses and "strains" by means of the following equation

$$\begin{Bmatrix} \tau_{sn} \\ \sigma_n \\ M \end{Bmatrix} = \begin{bmatrix} k_s & 0 & 0 \\ 0 & k_n & 0 \\ 0 & 0 & k_\omega \end{bmatrix} \begin{Bmatrix} \Delta u \\ \Delta v \\ \Delta \omega \end{Bmatrix} , \qquad (2.9)$$

where k_ω is obtained by assuming that closure along the joint is proportional to the force applied. The term $\Delta\omega$ is an incremental rotation and k_ω and M are defined later.

Goodman and St John assumed that joint closure at each nodal point pair I, L and J,K was proportional to the nodal point force there. (See Figure 2.3). When all the force is concentrated at nodal point I,L the relationship between the stiffness terms can be calculated as shown below.

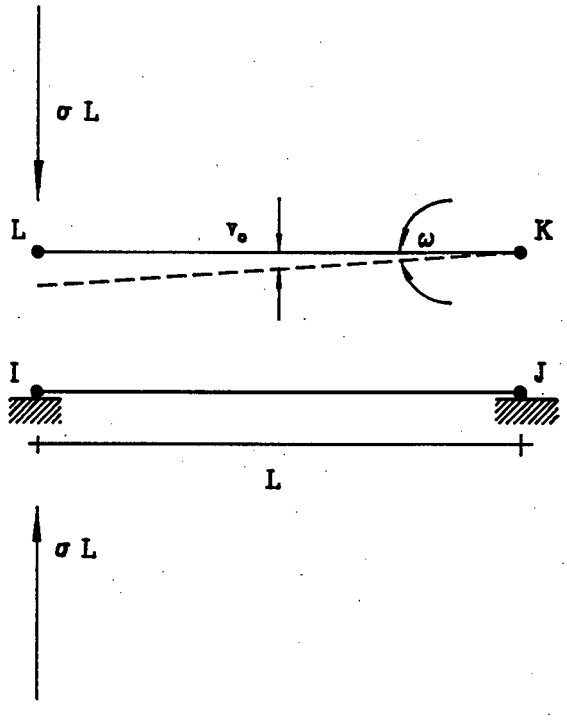

Calculation of rotational stiffness term.

FIG 2-3

If small strain theory is assumed,

$$\tan \omega \simeq \omega \qquad (2.10)$$

where ω is measured in radians. Then

$$\omega = \frac{2v_o}{L} , \qquad (2.11)$$

$$\frac{\sigma_n}{k_n} = v_o , \qquad (2.12)$$

and $$M_o = k_\omega . \omega = \frac{\sigma L^2}{2} . \qquad (2.13)$$

By successively eliminating v_o from equation (2.11) and σ from equation (2.13) we obtain a relation between rotational and normal joint stiffnesses

$$k_\omega = \frac{L^3 k_n}{4} \tag{2.14}$$

The inclusion of the rotation term causes the joint element to close and to pivot around the other node. This is because nodal-point closure is proportional to the nodal point force. The similar element without the rotation term, pivots around an internal point so that one end of the element closes and the other end opens.

A theoretical model formulated by Roberds and Einstein (1978) [7] represents elasto-viscoplastic behaviour of a discontinuity. In this model, invariant or non-oriented parameters are used. The octahedral normal stress σ_{oct}, expresses volumetric stress that leads to volumetric changes which are described by the volumetric strain, ϵ_{vol}. The maximum deviator stress describes the shear stress that leads to distortion which is, in turn, described by the maximum deviator strain, ϵ_{shear}.

The actual behaviour can be expressed as the sum of elastic and plastic behaviour. These can be considered as recoverable and unrecoverable parts respectively.

In terms of non-oriented parameters the elastic behaviour is given by

$$\begin{Bmatrix} \delta \epsilon^e_{vol} \\ \delta \epsilon^e_{shear} \end{Bmatrix} = [\, D^e \,] \begin{Bmatrix} \delta \sigma_{oct} \\ \delta 2q \end{Bmatrix} \tag{2.15}$$

where $[D^e]$ is the elastic material property matrix which is given by

$$[D^e] = \begin{bmatrix} 1/k^e & 0 \\ 0 & 1/G^e \end{bmatrix} \tag{2.16}$$

The parameters k^e and G^e are respectively the elastic bulk and deviatoric shear moduli.

The plastic behaviour can be expressed as

$$\begin{Bmatrix} \delta \epsilon^p_{vol} \\ \delta \epsilon^p_{shear} \end{Bmatrix} = [D^p] \begin{Bmatrix} \sigma_{oct} \\ 2q \end{Bmatrix} \tag{2.17}$$

in terms of non-oriented parameters where $[D^p]$, the plastic material property matrix, is defined as a function of stress ratio so that

$$\begin{Bmatrix} \delta \epsilon^p_{vol} \\ \hline \delta \epsilon^p_{shear} \end{Bmatrix} = f \left(\frac{\sigma_{oct}}{2q} \right) \tag{2.18}$$

One of the major advantages of using non-oriented parameters is a reduction of the computational effort to resolve the various principal strain orientations when a rotation of principal stresses occurs.

Yielding can be defined as a limiting stress state where elastic strains occur below the limit and plastic strains occur above the limit. Viscoplastic or time dependent behaviour occurs at a constant stress state and can also be expressed in non-oriented parameters as

$$\begin{Bmatrix} \delta \epsilon^{visco}_{vol} \\ \delta \epsilon^{visco}_{shear} \end{Bmatrix} = [D^{visco}] \delta t \tag{2.19}$$

where the material property matrix, $[D^{visco}]$ may be stress, strain or time dependent.

After a period of time yielding of the intact rock occurs and plastic behaviour starts. If the material is brittle this behaviour will be dilatant and strain-softening will occur in the intact rock. An instability which is associated with strain-softening can only be accommodated in a continuous medium by the creation of a discontinuity. It is then postulated that the yield surface of the intact rock will shrink towards the yield surface of the discontinuity. There are now two yield surfaces present in the rock mass - one for the intact rock and one for the discontinuity. As a result of stress redistribution, the discontinuity will behave elastically. Yielding will next occur when the yield stress of the discontinuity itself is exceeded. The behaviour of the joint will then be plastic and is assumed to be strain softening and dilatant.

As loading and unloading continues more and more asperities will shear off and the discontinuity yield surface will shrink to an ultimate residual yield surface. This surface may expand if the discontinuity is cemented by precipitates.

Pande (1979) [17] proposed an elasto-viscoplastic model which used Barton's empirical equation

$$\tau_p = \sigma_n \tan \left(JRC \log_{10} \left(\frac{JCS}{\sigma_n}\right) + \phi_b\right) \qquad (2.20)$$

to model the discontinuities. The yield function for the intact rock behaviour was expressed in invariant form as

$$F = F(\sigma_m , \bar{\sigma} , \theta_o) \qquad (2.21)$$

where σ_m = First invariant of stress

$\bar{\sigma}$ = $\sqrt{J_2}$, J_2 being the second deviatoric stress invariant

θ_o = Lodes angle.

By assuming the rock mass contains n joint planes and using Barton's experimental equation, the yield criteria for the k th joint was written as

$$F_k = [\ |\tau_k| + \sigma_{nk} \tan (JRC \log_{10} \frac{JCS}{\sigma_{nk}} + \phi_{bk}) \leq 0 \qquad (2.23)$$

In a multiaxial situation the total strain consists of elastic and viscoplastic parts. The elastic strain is related to stress by the matrix of elastic constants. The viscoplastic strain rates are non zero only if the stress state lies outside the yield surface and the strain rates and stresses are related via the viscoplastic flow rule. The total viscoplastic strain for the family of discontinuities is then written as

$$\dot{\underset{\sim}{\varepsilon}}^{vp} = \gamma_1 \langle F_1 \rangle \frac{\partial Q_1}{\partial \underset{\sim}{\sigma}} + \gamma_2 \langle F_2 \rangle \frac{\partial Q_2}{\partial \underset{\sim}{\sigma}} + \ldots\ldots$$

$$\ldots\ldots + \gamma_{n+1} \langle F_{n+1} \rangle \frac{\partial Q_{n+1}}{\partial \underset{\sim}{\sigma}} \qquad (2.24)$$

The function F was taken as linear and a non-associated flow rule was assumed (i.e. $Q \neq F$). In equation (2.24) the (n+1)-th term represents the yielding of the material matrix and the n-th term represents the appropriate yield function for the n-th family of weakness planes. A time history of stress and strain were found using various numerical integration techniques.

In order to cope with dilatancy, Pande proposed both an associated and non-associated flow rule. For the case of an associated flow rule the dilation angle is evaluated as

$$i = \tan^{-1} \left[\tan \lambda - \frac{JRC}{2.303} \sec^2 \lambda \right] \qquad (2.25)$$

where

$$\lambda = JRC \log_{10} (\frac{JCS}{\sigma_n}) + \phi_b \qquad (2.26)$$

Pande stated that the dilation angle obtained from equation (2.25) is considerably higher than that observed, so he proposed a damage coefficient M, greater than 1, which would scale down the dilatancy. The plastic potential function Q, could then be written as

$$Q = |\tau| + \sigma_n \tan\left[\frac{JRC}{M}\log_{10}\left(\frac{JCS}{\sigma_n}\right)\right] = 0 \qquad (2.27)$$

Heuze (1979) [18] & Heuze and Barbour (1982) [10] developed a new model to deal with axisymmetric interfaces and to describe the dilatant effects of rock joints. The material property matrix $\underline{k}$ was obtained in the conventional manner. The difficulty with zero thickness was overcome by assuming a non-zero thickness, t, and letting t tend to zero for the final calculation of $\underline{k}$.

The stress-strain relationship for the axisymmetric stresses and strains is

$$\begin{Bmatrix} \tau \\ \sigma_n \\ \sigma_\theta \\ \sigma_r \end{Bmatrix} = \begin{bmatrix} k_s t & 0 & 0 & 0 \\ 0 & k_n t & 0 & 0 \\ 0 & 0 & k_\theta \pi \bar{r} & 0 \\ 0 & 0 & 0 & k_r \ell \end{bmatrix} \begin{Bmatrix} \epsilon_s \\ \epsilon_n \\ \epsilon_\theta \\ \epsilon_r \end{Bmatrix} \qquad (2.28)$$

where θ = circumferential direction in the global system
k_s = shear stiffness
k_n = normal stiffness
k_θ = circumferential stretching stiffness
k_r = radial stretching stiffness.

In the final stiffness matrix, the two stretching stiffnesses k_θ and k_r will disappear as t tends to zero. In this approach all standard formulations for nodal forces due to initial stresses and strains can be used.

The model for joint dilation accounts for variable peak shear strength, shear stiffness and variable increase in normal stress as a function of the instantaneous dilation angle. Typical shear strength envelopes for rock joints are shown in Figure 2.4. The dilation angle, i, of the joint depends on the roughness of the joint and the normal pressure exerted on the joint.

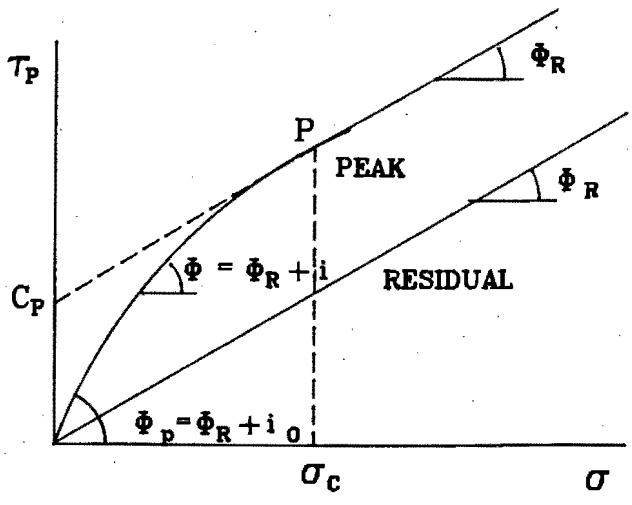

Shear strength envelopes for natural rock joints.

FIG 2-4

The peak dilation angle ϕ_p depends on the residual friction angle ϕ_r and the initial dilation angle i_o. As the normal stress is increased and the asperities are sheared off, the instantaneous dilation angle decreases until σ_c is applied. When the normal load is greater than σ_c no dilation takes place and the slope of the peak envelope equals the residual friction angle ϕ_r. A three parameter model was developed to describe the shear stress - normal stress relationship. The model was

$$\tau_p = A\sigma + B\sigma^2 + C\sigma^3 \qquad (2.29)$$

where $A = \tan \phi_p$

$$B = \frac{3C_p^*}{\sigma_c^2} - 2\,\frac{(\tan \phi_p - \tan \phi_r)}{\sigma_c}$$

$$C = -\frac{2C_p^*}{\sigma_c^3} + \frac{\tan \phi_p - \tan \phi_r}{\sigma_c^2} .$$

The instantaneous dilation angle is found by equating

$$\frac{d\tau}{d\sigma} = \tan (\phi_r + i) \qquad (2.30)$$

and equation (2.29) and rearranging δ is found to be

$$i = \tan^{-1} (A + 2B\sigma + 3C\sigma^2) - \phi_r \qquad (2.31)$$

and when $\sigma > \sigma_c$ the shear strength is given by the linear relationship

$$\tau_p = C_p^* + \sigma \tan \phi_r \qquad (2.32)$$

The model presented by Heuze for a dilatant joint estimates the change in normal joint stress for a given increment of shear displacement. A conceptual model with relevant parameters is shown below in Figure 2.5.

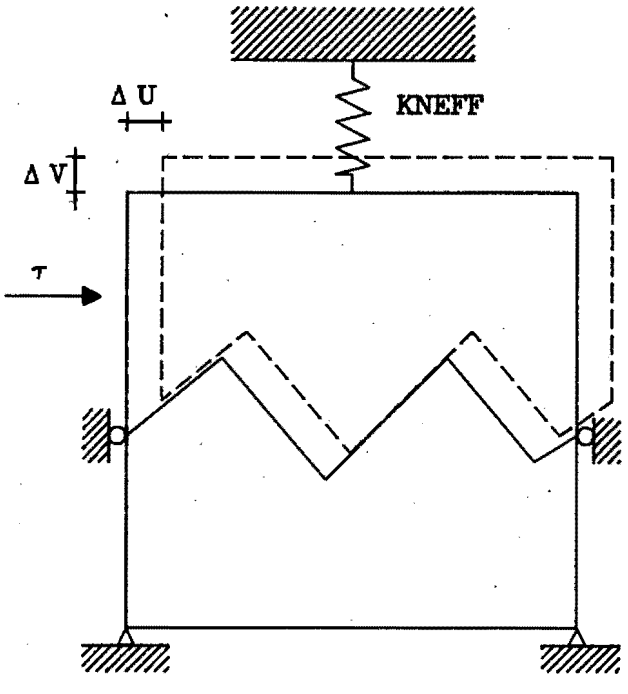

Conceptual model of a dilatant rock joint undergoing shear

FIG 2-5

KNEFF : stiffness of the adjacent structure transverse to the mean joint plane

k_n : normal stiffness of the joint

Δu : change in shear displacement along the joint

Δv : change in normal displacement across the joint

$\Delta \sigma$: increase in normal stress due to Δu .

The change in normal stress $\Delta\sigma$ is caused by a positive Δv which compresses the spring. However $\Delta\sigma$ also tends to reclose the joint which has a finite stiffness k_n. The normal opening of the joint can be expressed as

$$dv = \frac{\partial v}{\partial u} du + \frac{\partial v}{\partial \sigma} d\sigma \qquad (2.33)$$

where $\frac{\partial v}{\partial u} = \tan \delta$,

$$\frac{\partial v}{\partial \sigma} = -\frac{1}{k_n} \quad \text{(compression positive)},$$

and $$d\sigma = KNEFF.\ dv \ . \qquad (2.34)$$

By combining the above four equations an increment in normal stress can be found as a function of the shear displacement.

$$\Delta\sigma = \tan i \cdot \frac{k_n . KNEFF}{k_n + KNEFF} * \Delta u \ . \qquad (2.35)$$

Two problems were solved using this model and in each case, joints with and without dilation were compared. In the first case, the inclusion of dilation caused an increase in normal stress during shear displacement and in the second case, smaller displacements were predicted during movement of the rock mass.

2.4 CONCLUSIONS

The theoretical and empirical models presented here show some of the developments which have taken place in predicting the behaviour of jointed rock masses. The development of the finite element or "interface" type models has been traced. The initial four noded element and definition of the unit joint stiffnesses have been discussed. The use of isoparametric elements and the inclusion of rotation terms have also been dealt with. The models considered in this brief survey have provided an insight into the kinds of developments which have taken place in the modelling of joints. In all cases use is made of a specific element and some of the problems associated with the numerical formulation have been touched on. An alternative method of modelling joints can be achieved by treating the dislocation of joints as internal variables and applying the internal variable formulation of Martin [20].

This approach allows one to use a wide range of constitutive behaviours for the joints and these characteristics will be discussed later. The details of the internal variable formulation will be discussed in the next chapter.

CHAPTER 3

THEORY OF THE INTERNAL VARIABLE FORMULATION

3.1 INTRODUCTION

The theory of the internal variable formulation is derived from first principles in this chapter. The displacement and dislocation vectors and the "stress-strain" relationships are also defined. The ease with which the formulation can be adapted for use in a finite element program is shown. The various parts of the global stiffness matrix are derived and the assembly procedure is covered.

3.2 THE INTERNAL VARIABLE FORMULATION

The formulation used in this thesis is based on work done by Martin [20], [21]. The rock mass is considered to be a continuous domain split up into a finite element mesh. The displacements of the nodes can be given by a displacement vector $\underset{\sim}{u}$. The progressive displacements within the rock mass can be given by continuously changing the components of the vector $\underset{\sim}{u}$. The dislocations along a joint surface within the rock mass can be given by a vector $\underset{\sim}{\lambda}$.

The energy stored in a unit volume of the rock mass can be denoted by F , and is assumed to be a homogeneous quadratic function in terms of displacement $\underset{\sim}{u}$ and dislocation $\underset{\sim}{\lambda}$

$$F = F(\underset{\sim}{u}, \underset{\sim}{\lambda}) \tag{3.1}$$

This equation is essentially the Helmholtz free energy at constant temperature. The above equation is a potential function and can thus be rewritten as

$$dF = \frac{\partial F}{\partial \underset{\sim}{u}} d\underset{\sim}{u} + \frac{\partial F}{\partial \underset{\sim}{\lambda}} d\underset{\sim}{\lambda} \tag{3.2}$$

or alternatively

$$dF = \underset{\sim}{R}\, du - \underset{\sim}{X}\, d\lambda \tag{3.3}$$

In equation (3.3) the nodal forces $\underset{\sim}{R}$ and the internal forces acting on the dislocations $\underset{\sim}{X}$ are identified as

$$\underset{\sim}{R} = \frac{\partial F}{\partial \underset{\sim}{u}} \tag{3.4a}$$

$$\underset{\sim}{X} = -\frac{\partial F}{\partial \underset{\sim}{\lambda}} \tag{3.4b}$$

The minus sign in equation (3.4b) represents the forces being applied by the rock mass to the slips. Both $\underset{\sim}{R}$ and $\underset{\sim}{X}$ are homogeneous linear functions of $\underset{\sim}{u}$ and $\underset{\sim}{\lambda}$.

The dislocations $\underset{\sim}{\lambda}$ are associated with the internal forces $-\underset{\sim}{X}$ and the free or elastic strain energy can now be written as

$$F = \tfrac{1}{2}\, \underset{\sim}{u}^T \underset{\sim}{R} + \tfrac{1}{2}\, \underset{\sim}{\lambda}^T (-\underset{\sim}{X}) \tag{3.5}$$

and if

$$\underset{\sim}{R} = \underline{K}\, \underset{\sim}{u} + \underline{L}\, \underset{\sim}{\lambda} \tag{3.6a}$$

$$-\underset{\sim}{X} = \underline{L}^T \underset{\sim}{u} + \underline{H}\, \underset{\sim}{\lambda} \tag{3.6b}$$

The expression for the strain energy can now be rewritten as

$$F = \tfrac{1}{2}\, \underset{\sim}{u}^T \underline{K}\, \underset{\sim}{u} + \tfrac{1}{2}\, \underset{\sim}{u}^T \underline{L}\, \underset{\sim}{\lambda} + \tfrac{1}{2}\, \underset{\sim}{\lambda}^T \underline{L}^T \underset{\sim}{u} + \tfrac{1}{2}\, \underset{\sim}{\lambda}^T \underline{H}\, \underset{\sim}{\lambda} \tag{3.7}$$

In matrix form of the above equation is

$$F = \tfrac{1}{2} \begin{Bmatrix} \underset{\sim}{u} \\ \underset{\sim}{\lambda} \end{Bmatrix}^T \begin{bmatrix} \underline{K} & \underline{L} \\ \underline{L}^T & \underline{H} \end{bmatrix} \begin{Bmatrix} \underset{\sim}{u} \\ \underset{\sim}{\lambda} \end{Bmatrix}, \tag{3.8}$$

where $\underline{K}$ is the standard elastic stiffness matrix and the submatrices $\underline{L}$ and $\underline{H}$ will be defined in due course.

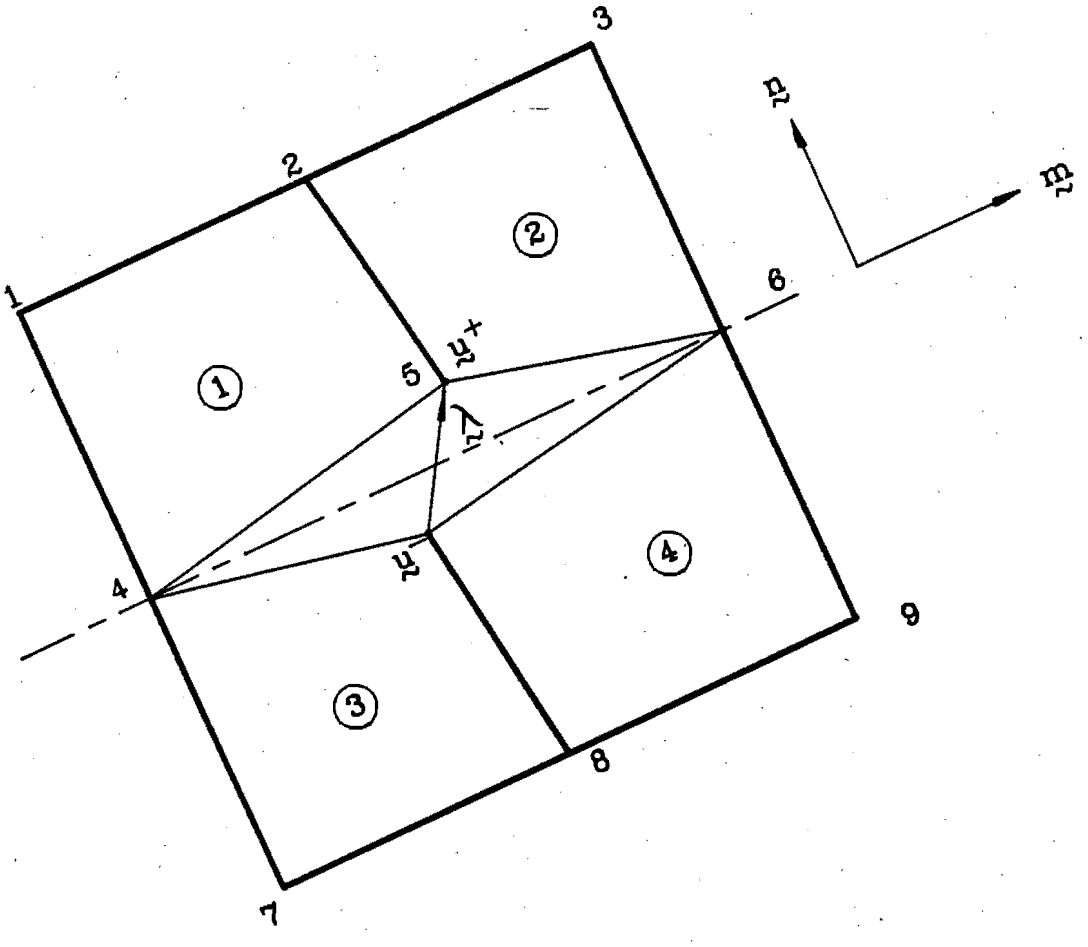

Finite element representation showing terms and vectors used in formulation.

FIG 3.1

In order to completely describe the mechanical behaviour of the rock mass, a kinetic relationship between the internal forces and the conjugate slip rates is required such that

$$\underset{\sim}{X} = X(\dot{\underset{\sim}{\lambda}}) \tag{3.9}$$

This relationship will be discussed in detail, in the next chapter.

In the problems we are dealing with, the loading, displacements and dislocations are all functions of time. Therefore, we can write the governing equations (3.6a) and (3.6b) as

$$\underset{\sim}{R}(t) = \underline{K}\,\underset{\sim}{u}(t) + \underline{L}\,\underset{\sim}{\lambda}(t) \tag{3.10a}$$

$$-\underset{\sim}{X}(t) = \underline{L}^{T}\,\underset{\sim}{u}(t) + \underline{H}\,\underset{\sim}{\lambda}(t) \tag{3.10b}$$

The above equations then describe the problem as rate dependent and t measures real time.

3.3 DEFINITIONS OF TERMS

The model assumes that slip occurs on a predefined slip surface. The slip surface is defined by tangential and normal vectors $\underset{\sim}{m}$ and $\underset{\sim}{n}$ respectively. The internal variable $\underset{\sim}{\lambda}$ is made up of shear and normal components λ_s and λ_n respectively and we write the dislocation as

$$\underset{\sim}{\lambda} = \lambda_s\,\underset{\sim}{m} + \lambda_n\,\underset{\sim}{n} \tag{3.11}$$

In Figure 3.1 a block of four elements has been shown with a dislocation line running through it and defined by $\underset{\sim}{m}$ and $\underset{\sim}{n}$. A dislocation has occurred at node 5 and two displacement parameters $\underset{\sim}{\lambda}$ and $\underset{\sim}{u}$ are active. The positive side of the slip line is that given by positive $\underset{\sim}{n}$. Therefore $\underset{\sim}{u}^{+}$ is the nodal displacement used in determining strains on the positive side of the slip line whereas $\underset{\sim}{u}^{-}$ is the nodal displacement used to determine strains on the negative side of the slip line.

The total nodal displacement can be written in terms of its positive and negative parts as

$$\underset{\sim}{u} = \frac{\underset{\sim}{u}^{+} + \underset{\sim}{u}^{-}}{2} \tag{3.12}$$

and the dislocation can be written as

$$\underset{\sim}{\lambda} = \underset{\sim}{u}^{+} - \underset{\sim}{u}^{-} \tag{3.13}$$

By combining equations (3.12) and (3.13), it follows that $\underset{\sim}{u}^{-}$ and $\underset{\sim}{u}^{+}$ can be written as

$$\underset{\sim}{u}^{-} = \underset{\sim}{u} - \tfrac{1}{2}\underset{\sim}{\lambda} \tag{3.14a}$$

$$\underset{\sim}{u}^{+} = \underset{\sim}{u} + \tfrac{1}{2}\underset{\sim}{\lambda} \tag{3.14b}$$

We are now in a position to identify the unknown matrices $\underline{L}$ and $\underline{H}$ from equation (3.8).

The strain energy contribution from each element to the global strain energy is given by

$$J_e = \tfrac{1}{2}\int_{V_e} \underset{\sim}{\sigma}^{T}\,\underset{\sim}{\epsilon}\,dV \tag{3.15}$$

where the integration is done over the volume of the element, V_e.

The strains $\underset{\sim}{\epsilon}$ and nodal displacements $\underset{\sim}{u}^{+}$ or $\underset{\sim}{u}^{-}$ are related by the strain-displacement matrix

$$\underset{\sim}{\epsilon} = \underline{B}\,\underset{\sim}{u}^{+}$$

or alternatively (3.16)

$$\underset{\sim}{\epsilon} = \underline{B}\,\underset{\sim}{u}^{-}$$

The rock mass behaviour is assumed to be elastic and the stress-strain relationship is given by

$$\underset{\sim}{\sigma} = \underline{D}\,\underset{\sim}{\epsilon} \tag{3.17}$$

If equations (3.14), (3.16) and (3.17) are combined, the stress can be rewritten as

$$\underset{\sim}{\sigma} = \underline{D}\,\underline{B}\,(\underset{\sim}{u} \pm \tfrac{1}{2}\,\underset{\sim}{\lambda}) \tag{3.18}$$

This, in turn, can be substituted into equation (3.15) which gives the elemental strain energy as

$$J_e = \tfrac{1}{2}\int_V (\underset{\sim}{u} \pm \tfrac{1}{2}\,\underset{\sim}{\lambda})^T\,\underline{B}^T\,\underline{D}\,\underline{B}\,(\underset{\sim}{u} \pm \tfrac{1}{2}\,\underset{\sim}{\lambda})\,dV \tag{3.19}$$

Expanding equation (3.19) gives

$$J_e = \tfrac{1}{2}\int_V [\,\underset{\sim}{u}^T(\underline{B}^T\,\underline{D}\,\underline{B})\,\underset{\sim}{u} \pm \underset{\sim}{u}^T(\tfrac{1}{2}\,\underline{B}^T\,\underline{D}\,\underline{B})\,\underset{\sim}{\lambda} \pm \underset{\sim}{\lambda}^T(\tfrac{1}{2}\,\underline{B}^T\,\underline{D}\,\underline{B})\,\underset{\sim}{u} + \underset{\sim}{\lambda}^T(\tfrac{1}{4}\,\underline{B}^T\,\underline{D}\,\underline{B})\,\underset{\sim}{\lambda}\,]\,dV \tag{3.20}$$

and when compared with equation (3.7), the form of matrices $\underline{K}$, $\underline{L}$ and $\underline{H}$ are clear.

$$\underline{K} = \int_V \underline{B}^T\,\underline{D}\,\underline{B}\,dV$$

$$\underline{L} = \pm\int_V \tfrac{1}{2}\,\underline{B}^T\,\underline{D}\,\underline{B}\,dV = \tfrac{1}{2}\,\underline{K} \tag{3.21}$$

$$\underline{H} = \int_V \tfrac{1}{4}\,\underline{B}^T\,\underline{D}\,\underline{B}\,dV = \tfrac{1}{4}\,\underline{K}$$

The sign of the contribution to the $\underline{L}$ matrix depends on which side of the slip line the element is located.

3.4 STIFFNESS MATRIX ASSEMBLY

In Figure 3.1, element 1 contributes a total symmetrical stiffness matrix $\underline{K}_1$ with submatrices $\underline{L}_1$ and $\underline{H}_1$ to the global stiffness matrix. The contributions to the $\underline{L}_1$ and $\underline{H}_1$ matrix are obtained directly from the $\underline{K}_1$ matrix, which is shown in equation (3.22)

$$\underline{K}_1 = \begin{bmatrix} a & a_2 & a_3 & a_4 & a_5 & a_6 & a_7 & a_8 \\ & b & b_3 & b_4 & b_5 & b_6 & b_7 & b_8 \\ & & c & c_4 & c_5 & c_6 & c_7 & c_8 \\ & & & d & d_5 & d_6 & d_7 & d_8 \\ & & & & e & e_6 & e_7 & e_8 \\ & & \text{SYM} & & & f & f_7 & f_8 \\ & & & & & & g & g_8 \\ & & & & & & & h \end{bmatrix} \qquad (3.22)$$

The dimensions of $\underline{L}_1$ and $\underline{H}_1$ will depend on the number of nodes of the element that are located on the slip line.

The $\underline{K}_1$ matrix is an 8 x 8 matrix corresponding to nodal displacements $\underset{\sim}{u}$ and nodal dislocations $\underset{\sim}{\lambda}$. It is assumed that the stiffness terms in equation 3.22 correspond to nodal displacements in element 1 starting from node 1 and continuing anti-clockwise. The $\underline{L}$ matrix is obtained by eliminating columns in this global matrix which correspond to nodal dislocations which are not on the slip line. The contribution to the $\underline{L}$ submatrix which is obtained from element 1 is thus

$$\underline{L}_1 = +\tfrac{1}{2} \begin{bmatrix} a_3 & a_4 & a_5 & a_6 \\ b_3 & b_4 & b_5 & b_6 \\ c & c_4 & c_5 & c_6 \\ c_4 & d & d_5 & d_6 \\ c_5 & d_5 & e & e_6 \\ c_6 & d_6 & e_6 & f \\ c_7 & d_7 & e_7 & f_7 \\ c_8 & d_8 & e_8 & f_8 \end{bmatrix} \qquad (3.23)$$

The positive sign denotes that element 1 is on the positive side of the slip line.

The contribution to the $\underline{H}$ submatrix is obtained in a similar manner. It is obtained by eliminating both the rows and columns associated with nodes not on the slip line. The corresponding $\underline{H}$ submatrix contribution from element 1 is therefore

$$\underline{H}_1 = \begin{bmatrix} c & c_4 & c_5 & c_6 \\ c_4 & d & d_5 & d_6 \\ c_5 & d_5 & e & e_6 \\ c_6 & d_6 & e_6 & f \end{bmatrix} \tag{3.24}$$

3.5 CONCLUSIONS

In this chapter it has been shown how the internal variable formulation can be used in finite element approximations. The numerical problems of ill-conditioning of the stiffness matrix caused by very high aspect ratios associated with distinct joint/interface elements are not encountered with the internal variable formulation.

An advantage of the internal variable formulation is the ease with which different constitutive laws for joint behaviour can be implemented without alterations to the rest of the formulation. Examples of these laws include elasto-plastic and viscoplastic behaviour of joints. A restriction which exists, however, is that one must be able to define how dislocations will change with time. In this study attention has been restricted to a viscoplastic constitutive law using a hyperbolic yield function. The implementation of this constitutive law will be discussed in the next chapter.

CHAPTER 4

THEORY OF VISCOPLASTIC BEHAVIOUR

4.1 INTRODUCTION

In order to model the behaviour of underground rock joints effectively, we require a constitutive law which will describe the behaviour of an underground rock joint. Observations in deep level mines have indicated that, in most instances, stope closure is time dependent and for this reason, a viscoplastic constitutive law is used.

4.2 BASIC ELASTO-VISCOPLASTIC EQUATIONS

The main assumption in viscoplasticity is that the inelastic strains in the material are developed with time. A rheological analogue of a viscoplastic material is shown in Figure 4.1.

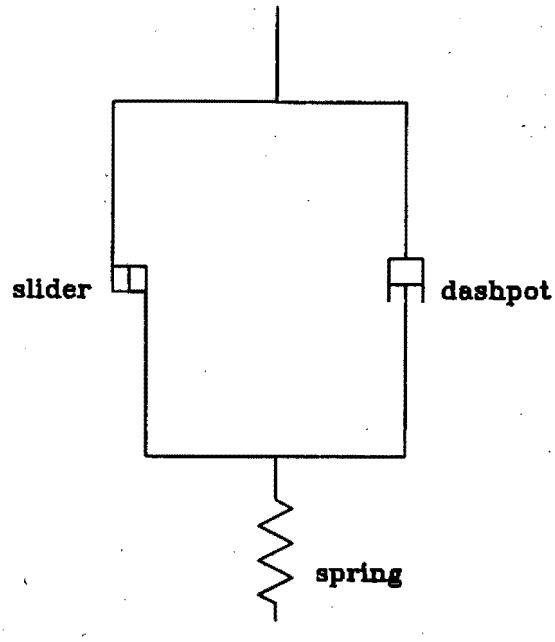

Rheological analogue of elasto-visco-plasticity.

FIG 4-1.

If, in a uniaxial test, a stress σ is applied to the material at time $t = 0$, the initial response of the material is elastic. If σ is less than the yield strength of the material, no inelastic strains occur. If, however, the applied stress is greater than the yield stress, viscoplastic strains take place at a certain finite rate $\dot{\epsilon}^{vp}$, the magnitude of which depends on how much greater the applied stress is than the yield stress. The stress-strain equations for this material are given by

$$\epsilon^{e} = \epsilon - \epsilon^{vp} \tag{4.1}$$

$$\sigma = E\,\epsilon^{e} \tag{4.2}$$

$$\sigma = E\,(\epsilon - \epsilon^{vp}) \tag{4.3}$$

The above equations are the same as those proposed by Pande *et al* [22].

Viscoplastic straining only occurs when the applied stress is greater than the yield stress. The stress response to an applied strain is shown in Figure 4.2. If a large enough strain is applied the induced stress will exceed the yield stress of the material. If the strain is held constant, the stress will relax to a steady state. The steady state is reached along the dotted lines. If unloading takes place, the viscoplastic strains remain permanent.

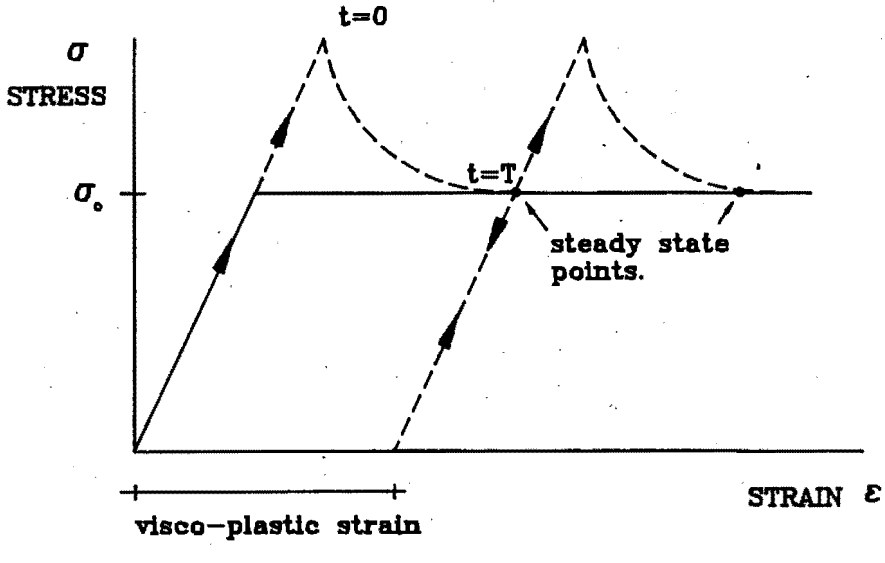

Stress-strain time history of elasto-visco-plastic material.

FIG 4-2

Certain aspects of viscoplastic theory are clear from Figure 4.2. Firstly, the material initially behaves elastically. Secondly, because stress trajectories can cross the yield surface, stress situations which violate the yield condition are possible. When a stress situation outside the yield surface occurs, a flow equation determines at what rate the stresses will return to the yield surface. The composition of the flow equation will be discussed next.

4.3 THE FLOW EQUATION

The slip rate on a joint is given explicity by

$$\dot{\underset{\sim}{\lambda}} = 1/\eta \; \langle \; \phi \; (F) \; \rangle \; \frac{\partial Q}{\partial \underset{\sim}{\sigma}} \qquad (4.4)$$

where $1/\eta$ is a fluidity parameter

$\phi \; (F) = F^n$ is the flow function

$F = F \; (\underset{\sim}{\sigma})$ is the yield function

Q is the plastic potential.

The angular brackets $\langle \; \rangle$ denote that the quantity within the brackets equals 0 if $F \leq 0$, or are treated as normal brackets if $F > 0$. It is also common for F to be raised to a power i.e. F^n . During the initial examples both n and $1/\eta$ were set equal to one for simplicity. Again, for simplicity, an associated flow rule was chosen so that $Q = F$. Equation (4.4) can now be written as

$$\dot{\underset{\sim}{\lambda}} = F \; (\underset{\sim}{\sigma}) \cdot \frac{\partial F}{\partial \underset{\sim}{\sigma}} \quad \text{for} \quad F \; (\underset{\sim}{\sigma}) \geq 0 \qquad (4.5)$$

$$\dot{\underset{\sim}{\lambda}} = 0 \quad \text{for} \quad F \; (\underset{\sim}{\sigma}) < 0 \qquad (4.6)$$

It was decided not to convert the nodal forces $\underset{\sim}{X}$ to stresses $\underset{\sim}{\sigma}$. It was considered to be more efficient and correct to use $\underset{\sim}{\lambda}$ directly associated with the conjugate forces $\underset{\sim}{X}$. The slip rates would then be derived directly from the conjugate forces. This meant that the flow equation would be written in terms of forces and not stresses as :

$$\dot{\underset{\sim}{\lambda}} = 1/\eta \; \langle \; F \; (\underset{\sim}{X}) \; \rangle \; \frac{\partial F}{\partial \underset{\sim}{X}} \qquad (4.7)$$

All that is required now is to define the form of the yield function $F(\underset{\sim}{X})$. The yield function that we use is a homogeneous, continuously differentiable function.

The function chosen was the hyperbolic function. This suited our purpose for two reasons. Firstly, it approximates the Mohr Coulomb yield criterion which has been extensively used in rock mechanics problems. Secondly, the singularity at the vertex point of the Mohr Coulomb yield criteria has been done away with because the hyperbola is continuously differentiable over its range. It is also comparable to the constitutive laws proposed by Patton [2], Ghaboussi *et al* [14], Heuze and Barbour [10] and the empirical law developed by Barton [15].

The general shape of a hyperbola is shown in Figure 4.3 where the axes are labelled X_n and X_s for normal and shear force respectively.

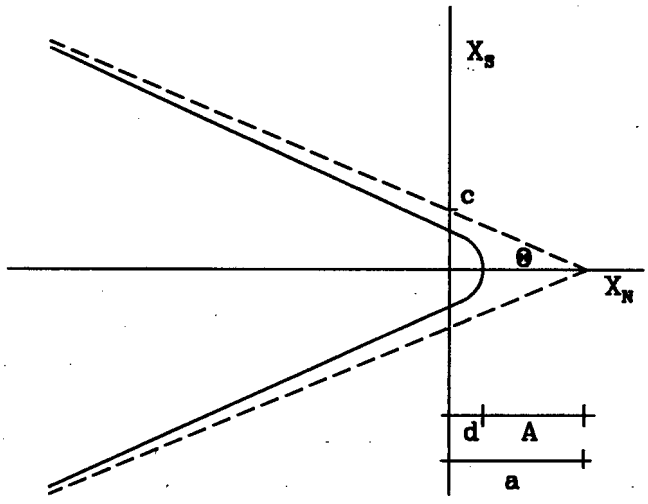

c = the cohesion
θ = angle for internal friction for the joints.
T = tan θ
a = c\T
A = parameter for locating the turning point of the yield surface.
d = a − A

The hyperbolic yield function.

FIG 4–3

4.4 THE FORMULATION OF THE HYPERBOLIC YIELD FUNCTION

The most general form of the hyperbola equation in terms of X_s and X_n is

$$F(\underset{\sim}{X}) = \frac{(X_n - a)^2}{A^2} - \frac{(X_s - b)^2}{B^2} \qquad (4.8)$$

This has the same form as the yield surface proposed by Zienkiewicz and Pande [23]. The function given in equation (4.8) was altered into a function which is homogeneous of degree one by using the approach taken by Eve, Reddy and Rockafellar [24]. The function in this form can easily be extended to elastic-plastic approaches, the discussion of which is beyond the scope of this thesis.

The yield condition is chosen such that when

$F(\underset{\sim}{X}) < 1$ elastic behaviour occurs

$F(\underset{\sim}{X}) = 1$ yielding occurs

and $F(\underset{\sim}{X}) > 1$ flow occurs.

It is necessary to relate the symbols used in Figure 4.3 to equation (4.8). By rearranging equation (4.8) and taking the limit as X_n tends to infinity, the constants A and B can be related to θ by

$$\tan\theta = \frac{B}{A} \qquad (4.9)$$

This resembles the Mohr-Coulomb yield condition where the constant θ is equivalent to the internal angle of friction. The line defined by equation (4.9) can be generalised by including an intercept on X_s axis, c . This is equivalent to a cohesion in the joint. It is important to note that the cohesion is expressed as a force and not as a stress.

If $a = A$, the cohesion can be taken as zero and by combining equations (4.8) and (4.9) the yield function can be written as

$$F(\underset{\sim}{X}) = (a - X_n) - \sqrt{\frac{X_s^2 A^2}{B^2} + a^2} \qquad (4.10)$$

The sign convention is chosen so that compression is negative and it is possible to have positive input and the correct signs for forces and their corresponding dislocation directions.

When cohesion is zero the slip rates can then be calculated using the following equation

$$\begin{Bmatrix} \dot{\lambda}_n \\ \dot{\lambda}_s \end{Bmatrix} = \left[(a - X_n) + \sqrt{\frac{X_s^2 A^2}{B^2} + a^2} \right] \begin{Bmatrix} -1 \\ -X_s A^2 \\ \hline B^2 \sqrt{\frac{X_s^2 A^2}{B^2} + a^2} \end{Bmatrix} \qquad (4.11)$$

In the case where the cohesion is not zero, equation (4.8) can be written as

$$F(\underset{\sim}{X}) = \frac{X_n^2}{A^2} - \frac{2a X_n}{A^2} + \frac{a^2}{A^2} - \frac{X_s^2}{\tan^2 \theta} \qquad (4.12)$$

This is once again changed to a homogeneous function of degree one and the following result is obtained

$$F(\underset{\sim}{X}) = \sqrt{(a^2 - A^2)} - \frac{X_n a}{\sqrt{(a^2 - A^2)}} - \sqrt{\frac{X_s^2}{\mathrm{Tan}^2 \theta} + \frac{X_n^2 A^2}{(a^2 - A^2)}} \qquad (4.13)$$

As in the previous case the directions of dislocation are given by the derivatives of $F(\underset{\sim}{X})$.

The yield surface is convex, i.e. a line joining only two stress points within or on the yield surface would lie completely inside or on the yield surface (see Martin [25]). The restrictions placed on the direction of viscoplastic straining or the normality rule were satisfied.

A possible improvement on the present constitutive model would be to implement a non-associated flow rule. This would allow a change of the dilation angle to occur where the change would be dependent on the normal force across the joint. If the initial internal angle of friction of ϕ_o is made up of ϕ_r and δ_o which are the residual friction angle and the initial dilatancy angle respectively, as the normal force increases, δ_o would decrease to zero and therefore ϕ_o would decrease to ϕ_r . The point at which ϕ_o would equal ϕ_r would depend on the yield shear strength of the adjacent rock.

Another development along similar lines would be to allow closing to take place by allowing the dilation angle δ to become negative. This could possibly be done by entering an asperity height and length and comparing the relative displacements of the joint sides with the asperity dimensions entered. If the movement of the joint exceeds the asperity dimensions at a stress below the yield stress of the rock, the dilatancy angle would become negative and closure would take place. The material properties of the intact rock would then dictate any subsequent behaviour of the rock mass. These suggestions could form the basis of further work to improve the performance of the model. Time restrictions did not permit the inclusion of these refinements.

4.5 CONCLUSIONS

In this chapter we have discussed a viscoplastic constitutive law which relates the slip rate on the joints to the conjugate forces. Special attention has been paid to the yield function associated with the viscoplastic equations and a continuous homogeneous function of degree, one which resembles the Mohr-Coulomb yield condition, has been chosen. Possible extensions which could be applied to the constitutive behaviour were also suggested.

What is required now is a method for progressively monitoring the evolution of dislocations and forces which occur on discontinuities. A time stepping algorithm is needed for this purpose and in the next chapter various time integration schemes will be discussed.

CHAPTER 5

IMPLICIT AND EXPLICIT TIME STEPPING ALGORITHMS

5.1 INTRODUCTION

When using viscoplasticity, it is necessary to use a time marching scheme in order to trace the changes in the primary and secondary variables as time progresses. There are two main types of time integration techniques, namely forward difference or explicit schemes and backward difference or implicit schemes. The theory of each type will be discussed in this chapter and the drawbacks and benefits of each scheme will be covered.

5.2 EXPLICIT TIME INTEGRATION ALGORITHM

The Euler forward scheme is a very simple one step method of a time marching procedure that does not require any iterations. As a result, the only decision the user has to make when applying this algorithm involves the time step length. For stability reasons explicit algorithms need a large number of small time steps. The cost of a large number of time steps is, however, offset by the low cost of each explicit step.

For our problem, it is assumed that at a particular point in time, say $t = t_{n-1}$, a solution for the governing equations (3.10a) and (3.10b) given in chapter 3 is known. In order to maintain global equilibrium the internal forces $\underset{\sim}{R}$, are set equal to applied forces $\underset{\sim}{P}$. These applied forces are regarded as functions of time and therefore it is possible to write

$$\underline{\underline{K}}\, \underset{\sim}{u}_{n-1} + \underline{\underline{L}}\, \underset{\sim}{\lambda}_{n-1} = \underset{\sim}{P}_{n-1} \tag{5.1a}$$

$$\underline{\underline{L}}^{T}\, \underset{\sim}{u}_{n-1} + \underline{\underline{H}}\, \underset{\sim}{\lambda}_{n-1} = -\underset{\sim}{X}_{n-1} \tag{5.1b}$$

The displacements, dislocations and forces are all functions of time. It is necessary to advance to the next step, $t = t_n$. The slip rate $\dot{\underset{\sim}{\lambda}}_{n-1}$ which has been calculated from the flow rule at the end of the n-1th step, is now used to approximate the incremental slip $\Delta\lambda$ for nth step.

We can therefore write

$$\Delta\underset{\sim}{\lambda} = \Delta t \ \dot{\underset{\sim}{\lambda}}_{n-1} \tag{5.2}$$

where

$$\dot{\underset{\sim}{\lambda}}_{n-1} = \frac{1}{\eta} F(\underset{\sim}{X}_{n-1}) \left.\frac{\partial F}{\partial \underset{\sim}{X}}\right|_{n-1} \tag{5.3}$$

At this point everything except the displacements in equation (3.9a) is known and this can easily be evaluated by solving the following equation

$$\underline{\underline{K}}\Delta\underset{\sim}{u} = \underset{\sim}{P}_n - \underset{\sim}{P}_{n-1} - \underline{\underline{L}}(\underset{\sim}{\lambda}_{n-1} + \Delta\underset{\sim}{\lambda}) - \underline{\underline{K}}\underset{\sim}{u}_{n-1} \tag{5.4}$$

These displacements are substituted into equation (3.9b) to solve for the internal nodal forces $-\underset{\sim}{X}_n$, which are used in the yield function to calculate the slip rate at the end of the step in readiness for the next time increment. This method is very simple and easily implemented and because the rock mass is assumed to respond elastically, and hence no iterations are required. It suffers from the major drawback of instability if the time step length is not sufficiently small.

5.3 IMPLICIT TIME STEPPING ALGORITHM

Although implicit schemes are more complicated than explicit schemes, they do have some advantages. Geradin *et al* [26] gave a comprehensive survey of implicit schemes which have been used in finite element methods.

Implicit programs are often more general than explicit programs. The time step length is not as strongly limited by stability considerations and therefore the cost of one time step is not a critical criterion of performance. When applied to linear problems implicit codes are neither more difficult to apply or implement than explicit codes and the only additional cost is the linear solution of equations involved at each iteration.

In nonlinear systems however several choices have to be made so that the accuracy of the solution can be controlled. These would include a method for iterating within a time step and the choice of time step length which would depend on the convergence of the iteration procedure within the time step.

In the application of the implicit integration scheme to our problem, the following algorithm discussed by Owen & Hinton [27] and Kanchi *et al* [28] and Zienkiewicz [29] was used

$$\Delta\underset{\sim}{\lambda} = \Delta t \left[(1 - \Theta) * \underset{\sim}{\lambda}^{\bullet c}_{n-1} + \Theta * \underset{\sim}{\lambda}^{\bullet p}_{n} \right] \qquad (5.5)$$

where $\Delta\underset{\sim}{\lambda}$ = dislocation increment

Δt = time step length

β = constant for particular integration scheme ($0 \leq \beta \leq 1$)

$\underset{\sim}{\lambda}^{\bullet c}_{n-1}$ = corrected slip rate at end of previous time step

$\underset{\sim}{\lambda}^{\bullet p}_{n}$ = predicted slip rate for end of present time step.

The value of the constant Θ can vary between 0 and 1. If $\Theta = 0$, the Euler forward or fully explicit method is recovered since the dislocation increment is completely determined from conditions existing at time $t = t_{n-1}$. If $\Theta = 1$, a backward difference or fully implicit scheme is employed with the dislocation increment being determined from the slip rate corresponding to the end of the time interval. If $\Theta = \frac{1}{2}$, the implicit trapezoidal or Crank-Nicholson scheme is used.

For any value of $\Theta > 0$, it is necessary to use a predictor-corrector solution procedure because "unknown" values of the slip rate are used on the righthand side of equation (5.4).

If a solution to the problem is known at $t = t_{n-1}$, equations (5.1a) and (5.1b) again hold. The dislocation increment is calculated from equation (5.4) using a proportion of $\underset{\sim}{\lambda}^{\bullet c}_{n-1}$ and $\underset{\sim}{\lambda}^{\bullet p}_{n}$, depending on the value of Θ used. The predicted slip rate $\underset{\sim}{\lambda}^{\bullet p}_{n}$ is then compared to the corrected slip rate $\underset{\sim}{\lambda}^{\bullet c}_{n}$, which is calculated from the yield function. If these two slip rates are close enough, ie. within some preset tolerance, $\underset{\sim}{\lambda}^{\bullet c}_{n}$ becomes the slip rate and is used as an initial prediction for the slip rate at the end of the next or n+1th time step. If the two slip rates are not within the given tolerance, $\underset{\sim}{\lambda}^{\bullet p}_{n}$ is set equal to $\underset{\sim}{\lambda}^{\bullet c}_{n}$ and the solution procedure is repeated until either convergence is obtained or the maximum number of iterations for the time step is exceeded. This method was used by Zienkiewicz and Cormeau [30].

The explicit procedure is not only simple in its method of advancing with time but also in its way of coping with displacements, dislocations and internal forces which are simply updated with each time step. The implicit procedure is more complicated in that it requires both the corrected and the predicted incremental values of dislocations, slip rates, displacements, conjugate forces and strains to be stored in memory.

5.4 TIME STEP LENGTH

It is well known that explicit integration schemes suffer from numerical instability when the time step length is too big. Much attention has been given to the time stepping strategy as this governs efficiency and accuracy. If the time step is too large the accuracy suffers and instability may occur. If the time step is too small the expense of

solving the problem may be excessive. Levy and Pifko [3] based their criterion for stability on the total strain

$$\Delta t = \tau \frac{\bar{\epsilon}_{Total}}{\bar{\epsilon}^{c}} \tag{5.6}$$

where τ varied from 0.10 to 0.15.

Fritz [32] used the same stability limit but he found that control over accuracy and stability could only be gained by reducing the time interval.

The above work was derived from stability analysis done by Ziekiewicz and Cormeau [30]. Cormeau [33] presented a formula for determining the critical time step length, Δt_c for Mohr-Coulomb type materials. This formula is given by

$$\Delta t_c = \frac{(1 + \nu)\ (1 - 2\nu)\ F_o}{\gamma E\ (1 - 2\nu + \sin^2\theta)\ \Psi'} \tag{5.7}$$

where ν and E are elastic material constants, θ is the internal angle of friction and F_o is a normalising constant to the yield function. The constants γ and Ψ' are set equal to one for the sake of simplicity. It is important to note that this stability limit is independent of the finite element mesh subdivision. The above stability limit was used in subsequent examples.

5.5 CONCLUSIONS

In this chapter we have briefly discussed explicit and implicit time integration schemes which can be used to determine the time-dependent response of rock joints. The explicit algorithm was considered separately and certain advantages highlighted. A general implicit time integration scheme was discussed and the relationship with the explicit

scheme pointed out. Various factors concerning stability of the schemes and iterative procedures were also discussed. In the next chapter some numerical examples are presented which illustrate some of the above features.

CHAPTER 6

ILLUSTRATIVE NUMERICAL EXAMPLES

6.1 INTRODUCTION

In the preceding chapters, the internal variable formulation, viscoplastic constitutve law and various integration schemes were discussed. These features were all included in the 2-D finite element program NOSTRUM, which was developed for research purposes in the Centre for Research in Computational and Applied Mechanics (CERECAM). In order to test the validity of the program a series of numerical examples were conducted and these will be discussed in some detail in this chapter.

6.2 PLANE STRAIN "BLOCK"

In order to test that the program was giving correct results, a simple problem involving two plane strain elements was chosen. The reason for this choice is that it is possible to obtain an analytical solution for comparison purposes. The element layout, boundary conditions and material properties are given in Figure 6.1.

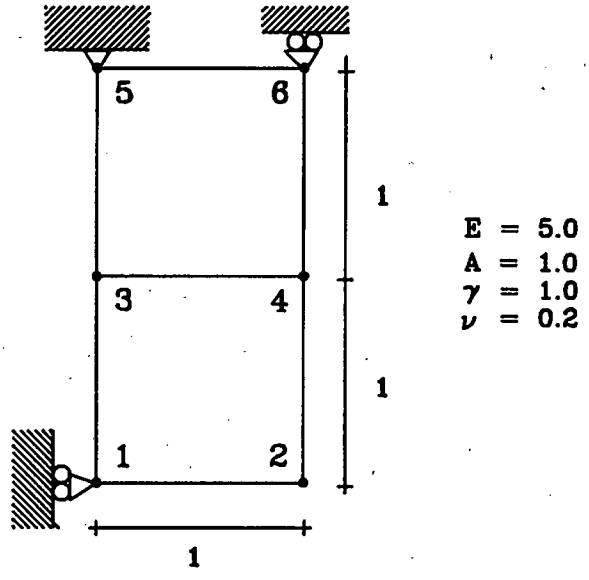

Finite element mesh for initial program tests.

FIG 6-1

There is a horizontal joint between nodes 3 and 4. The model was pinned at node 5 and on rollers at nodes 1 and 6. This enabled any internal stresses built up during loading to be dissipated as time progressed.

An initial downwards vertical displacement of 0.2 was applied at nodes 1 and 2. With the viscoplastic yield function, as the time tended to infinity, the normal dislocation across the joint would approach the initially applied displacement as time tended to infinity. The tangential slip across the joint in this case would be negligible as relaxation takes place.

The analytical solution required to verify the results obtained is discussed below. The relaxation was modelled using the rheological model consisting of two springs and a dashpot as shown in Figure 6.2.

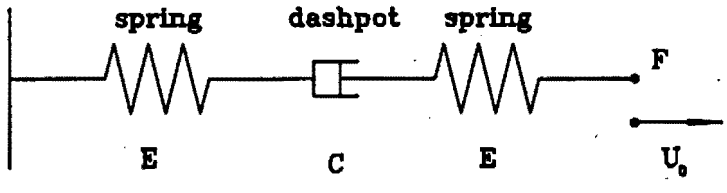

Rheological analogue for analytical solution.

FIG 6-2.

The total displacement u in the system is given by

$$u = \frac{2F}{E} + \lambda \qquad (6.1)$$

where E = spring stiffness
F = applied force
λ = dislocation across the joint (or dashpot)
C = viscosity of the dashpot.

The dislocation rate across the joint can be modelled by

$$\dot{\lambda} = CF \tag{6.2}$$

where C is a constant obtained from the constitutive law.

By differentiating equation (6.1) and combining it with equation (6.2) the following equation is obtained

$$\dot{F} + \frac{EFC}{2} = 0 \tag{6.3}$$

The boundary conditions, initial conditions and end conditions which were applied are as follows

$$u(o) = u_o \quad \text{(initial applied displacement)}$$
$$\dot{u}(t) = 0 \quad \text{for} \quad t > 0$$
$$\lambda(o) = 0$$
$$F(o) = \frac{Eu_o}{2}$$

By solving equation (6.3) and applying the appropriate boundary conditions the solution for force dissipation across the joint was found. The solution was

$$F(t) = \frac{Eu_o}{2} e^{-\frac{ECt}{2}} \tag{6.4}$$

This solution was substituted into equation (6.2) and the following relationship between dislocation of the joint and time was obtained.

$$\lambda(t) = u_o \left[1 - e^{-\frac{ECt}{2}}\right] \tag{6.5}$$

By substituting values for E, C and u_o into equations (6.4) and (6.5), it was possible to compare the results obtained from the analytical equations with the finite element approximations. These comparisons are shown in Figure 6.3 and Figure 6.4.

The normal dislocation across the joint converges to the expected value of 0.2 as the material relaxes viscoplastically. The normal force decreases to zero as time tends to infinity.

The various methods of integration are compared in the graphs. These are shown in Table 6.1.

Type	β
Explicit	0.0
Crank Nicholson	0.5
Galerkin	0.6667
Implicit	1.0

INTEGRATION TYPES USED IN ANALYSES.

TABLE 6.1

The integration factor, β , given in Table 6.1 relates to the algorithm discussed in Chapter 5. From Figures 6.3 and 6.4 certain aspects of the numerical procedure are shown. The different integration schemes clearly approximate the analytical solution. The explicit integration scheme overpredicts the slips and forces. The implicit schemes progressively underpredict the slips and forces when compared to the analytical results. The Crank-Nicholson integration scheme is the closest approximation to the analytical solution. It was for this reason that the Crank-Nicholson integration scheme was used in the more complicated examples presented later in this chapter.

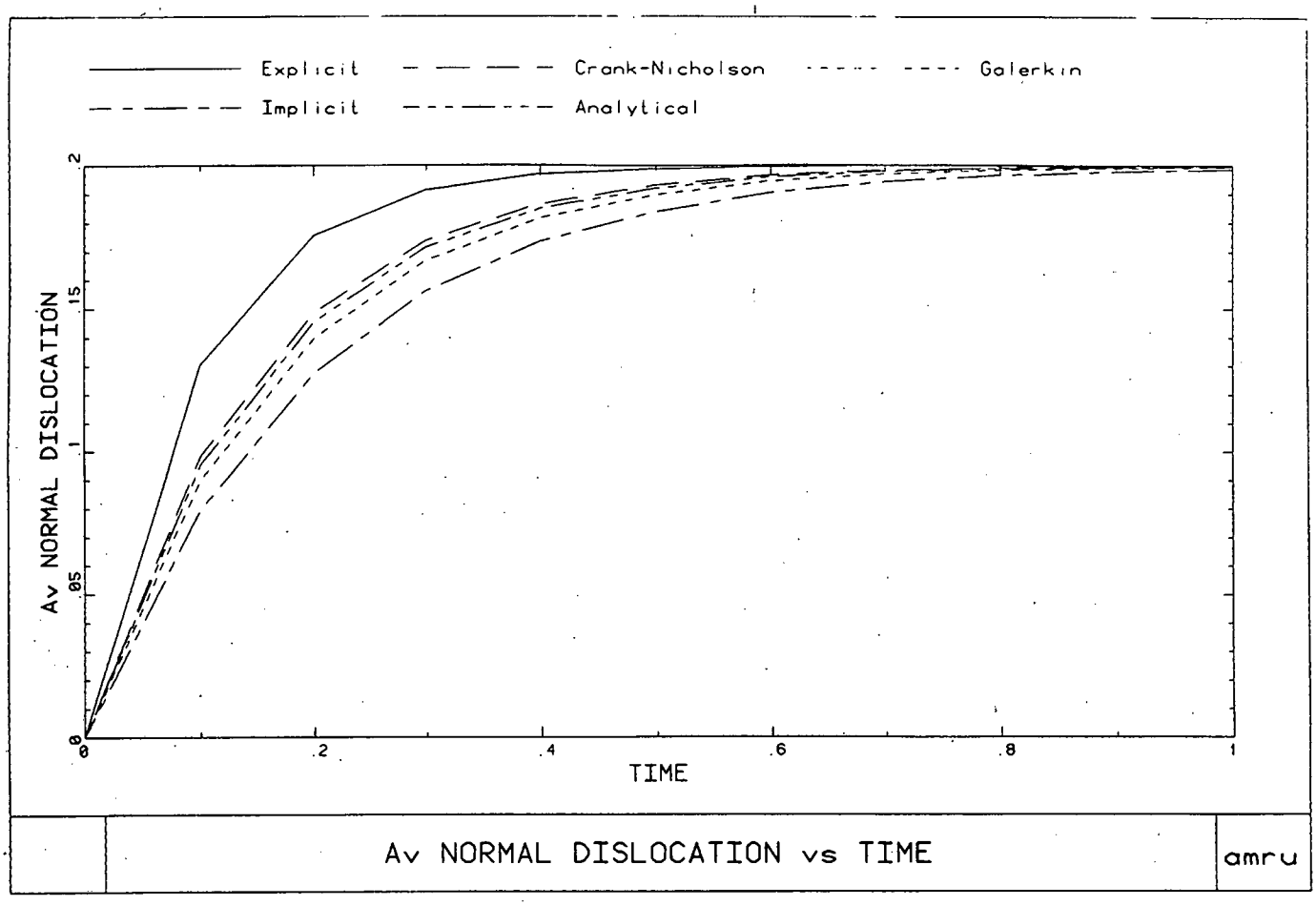

FIG 6–3 Plane strain 'block' model.
Normal dislocation versus Time.

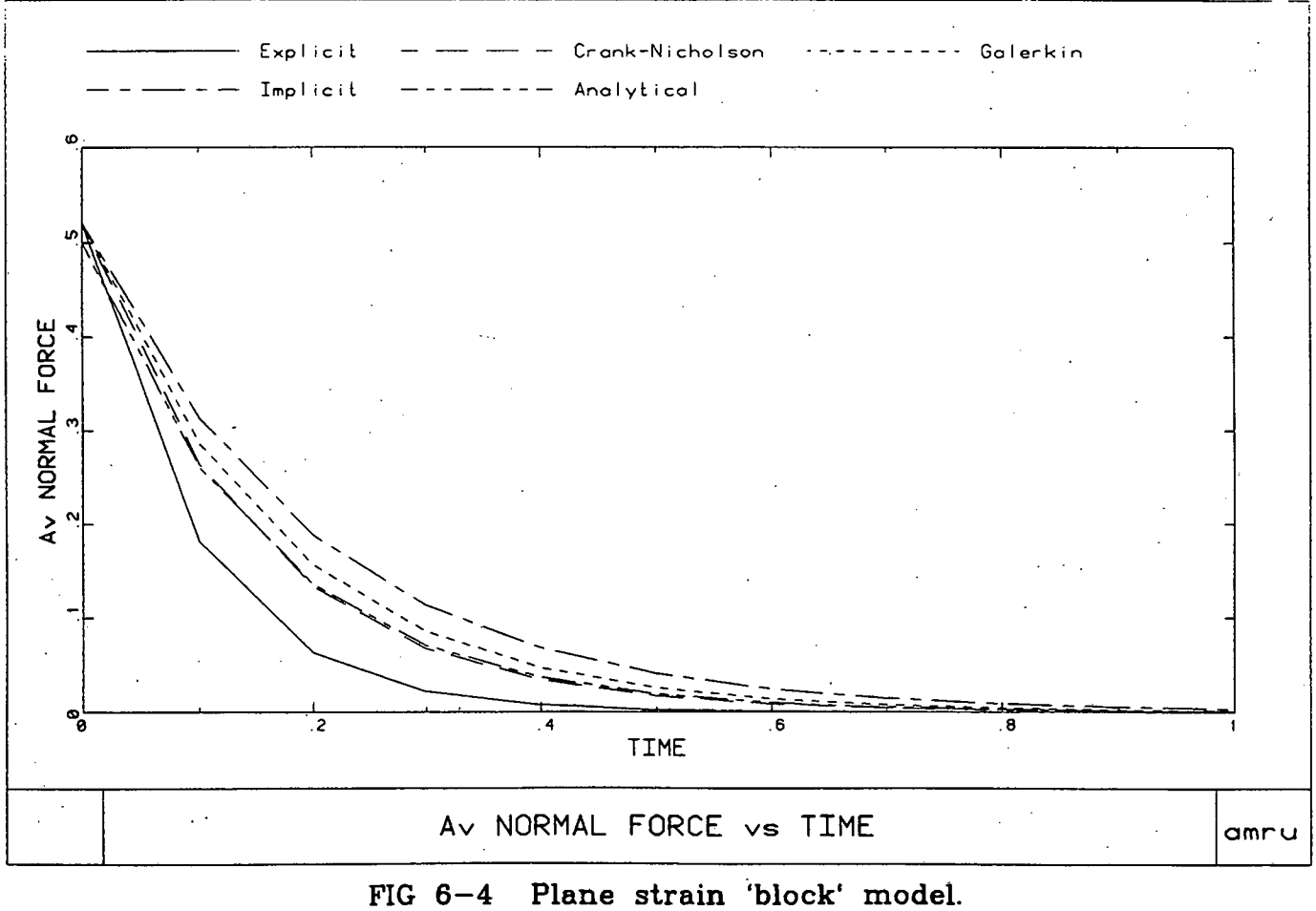

FIG 6–4 Plane strain 'block' model.
Normal force versus Time.

In the above example, the yield function was altered in order to give the desired results. A steep, near vertical yield surface was required when modelling the normal dislocation. This was achieved by using relatively large values for the apparent cohesion and the internal friction angle. This dictated that the direction of slip would be predominantly in the normal direction.

6.3 BEAM EXAMPLES

It was now possible to model the behaviour of more practical examples. The following series of examples consider the more practical problem of beams with vertical slip lines. A question which has been receiving considerable attention is that of what causes the observed compressive stresses in the hangingwall beam in deep level mines. A number of mechanisms have been proposed to explain this phenomenon but none have been conclusive. These examples illustrate another mechanism which can contribute to the horizontal stresses developed in the beam.

6.3.1 Beam with single slip line

The first example we consider is a beam with a single slip line. The finite element mesh was refined vertically by increasing the number of nodes on the slip line. By comparing the results obtained from the three meshes it was possible to choose a mesh which gave acceptable results in a reasonable time. The finite element meshes are shown in Figure 6.5, 6.6 and 6.7. All the meshes have the same overall dimensions and a vertical joint 0.25 m from the fully fixed end. The values of Young's Modulus and Poisson's ratio used were 70×10^9 Pa and 0.2 respectively. These are representative values commonly quoted in the literature by Lama [34], Stagg and Zienkiewicz [35] and Jaeger and Cook [36]. Brummer [37], [38] believes that the hangingwall (roof) and the footwall (floor) of the stope are passive, loose layers of rock. Therefore the only imposed loading was the selfweight of the beam. The density of the rock was taken as 2700 kg/m^3 and this was applied linearly over a number of time steps. The

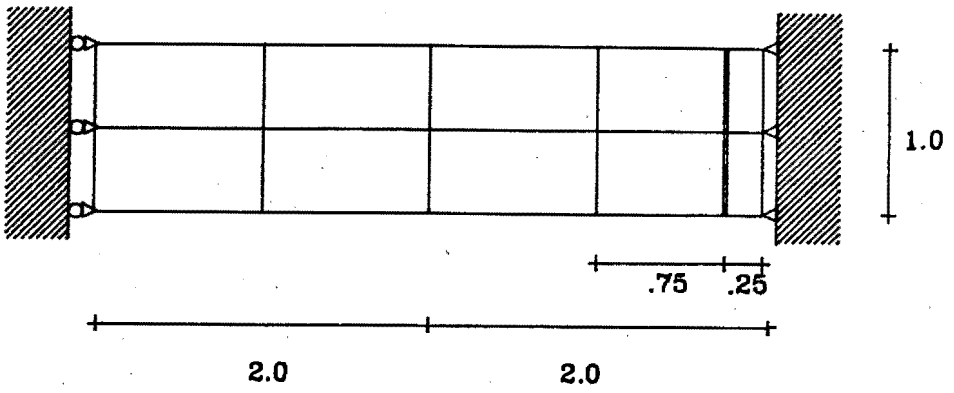

Finite element mesh for hanging wall beam
– 10 element mesh, 3 slip nodes.

FIG 6–5

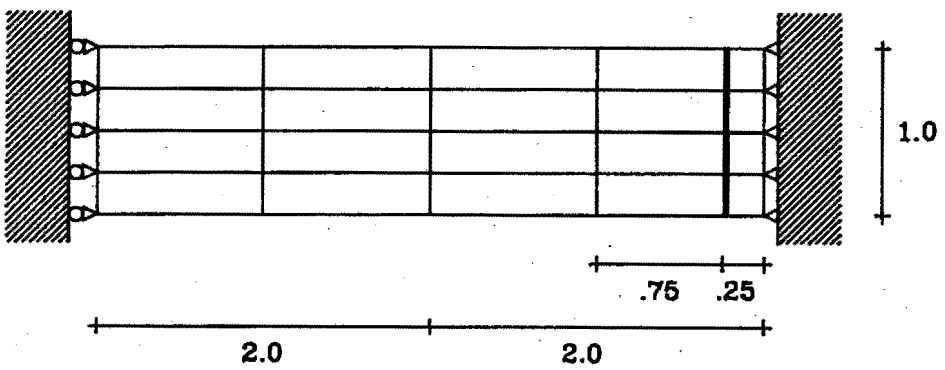

Finite element mesh for hanging wall beam
– 20 element mesh, 5 slip nodes.

FIG 6–6

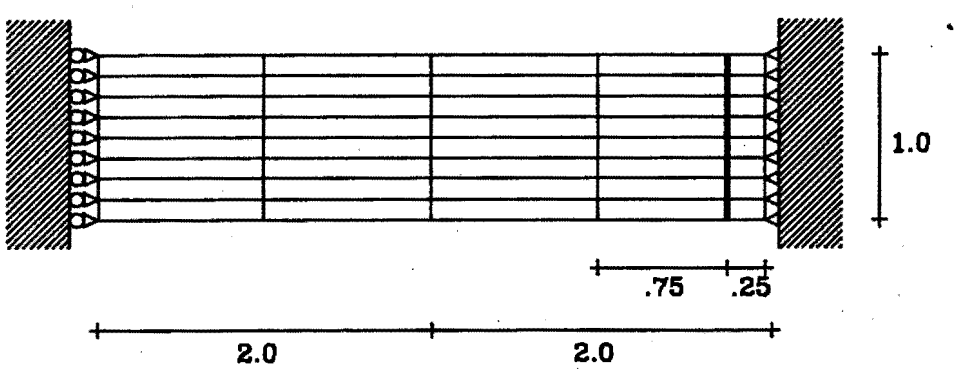

Finite element mesh for hanging wall beam
– 40 element mesh, 9 slip nodes.

FIG 6–7

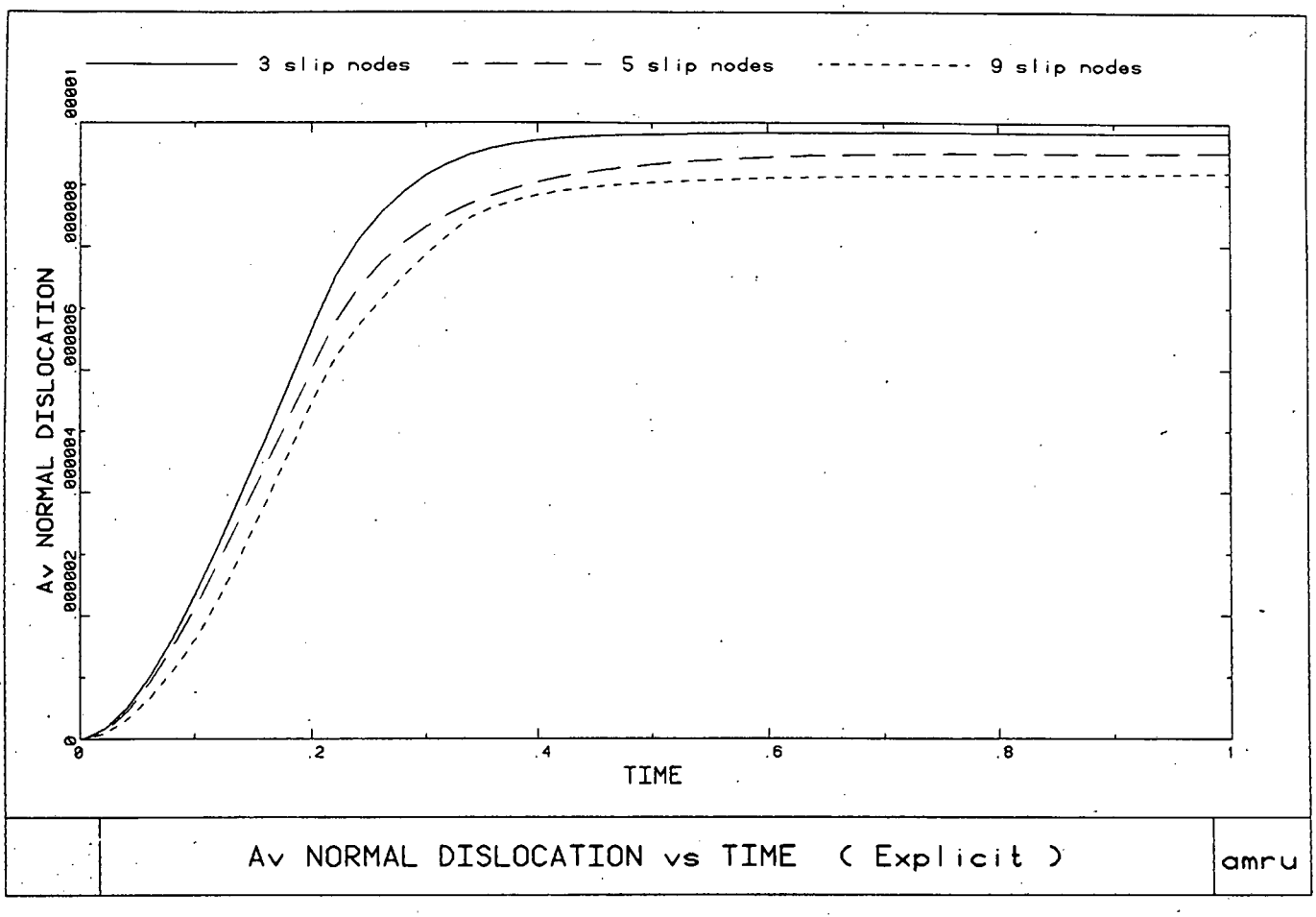

FIG 6–8 Average normal dislocation versus Time. Explicit Integration.

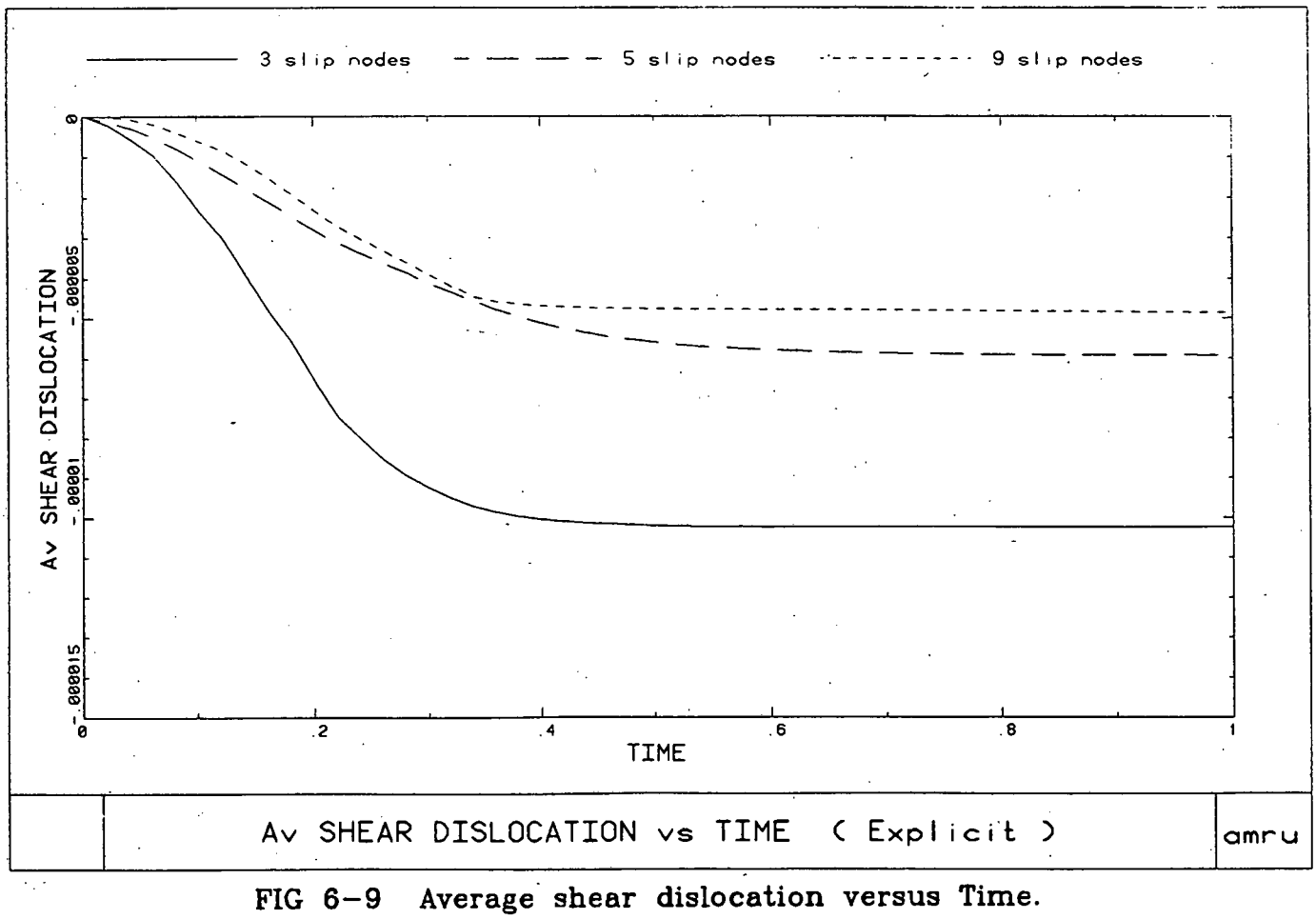

FIG 6–9 Average shear dislocation versus Time. Explicit Integration.

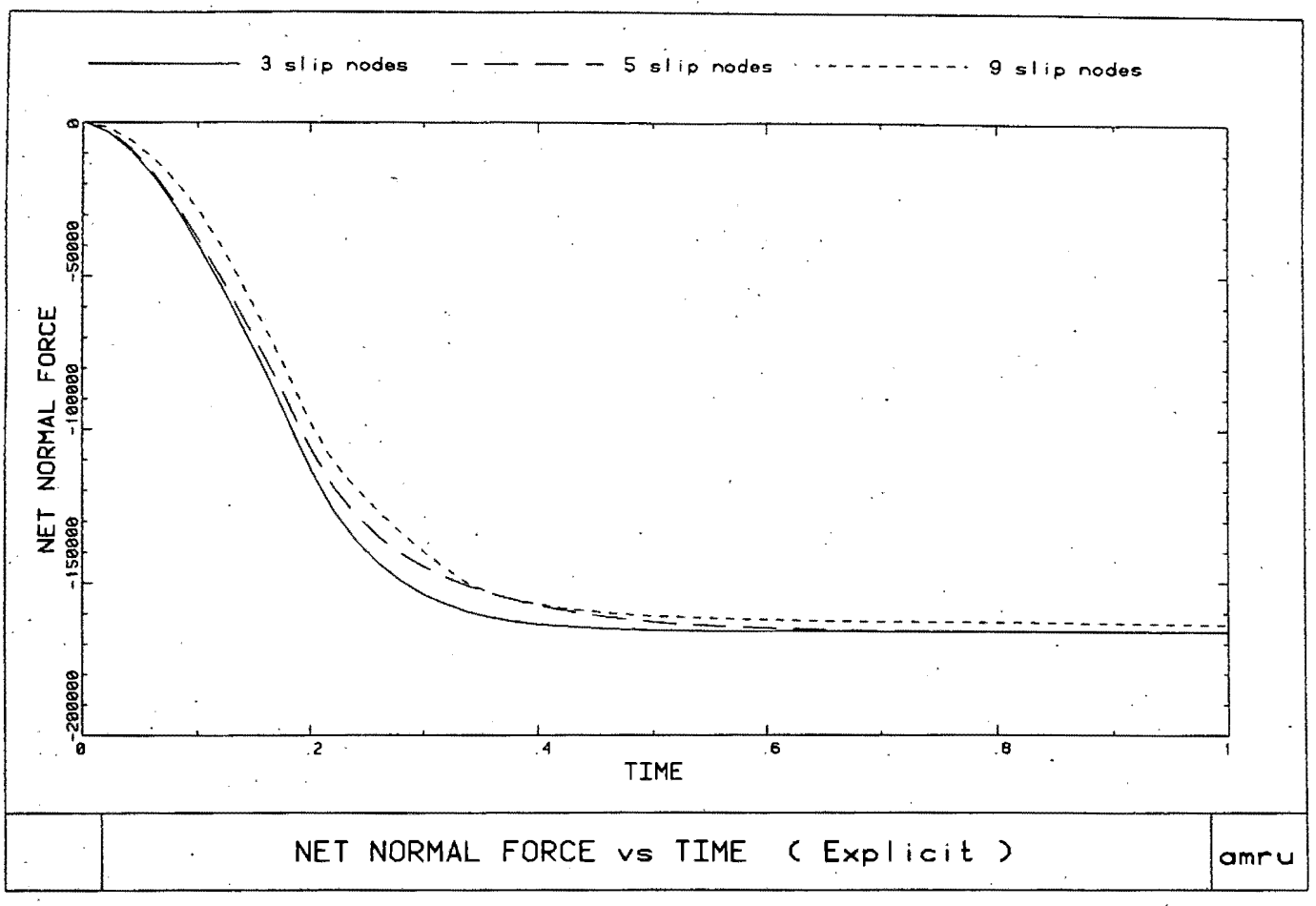

FIG 6–10 Net normal force versus Time.
Explicit Integration.

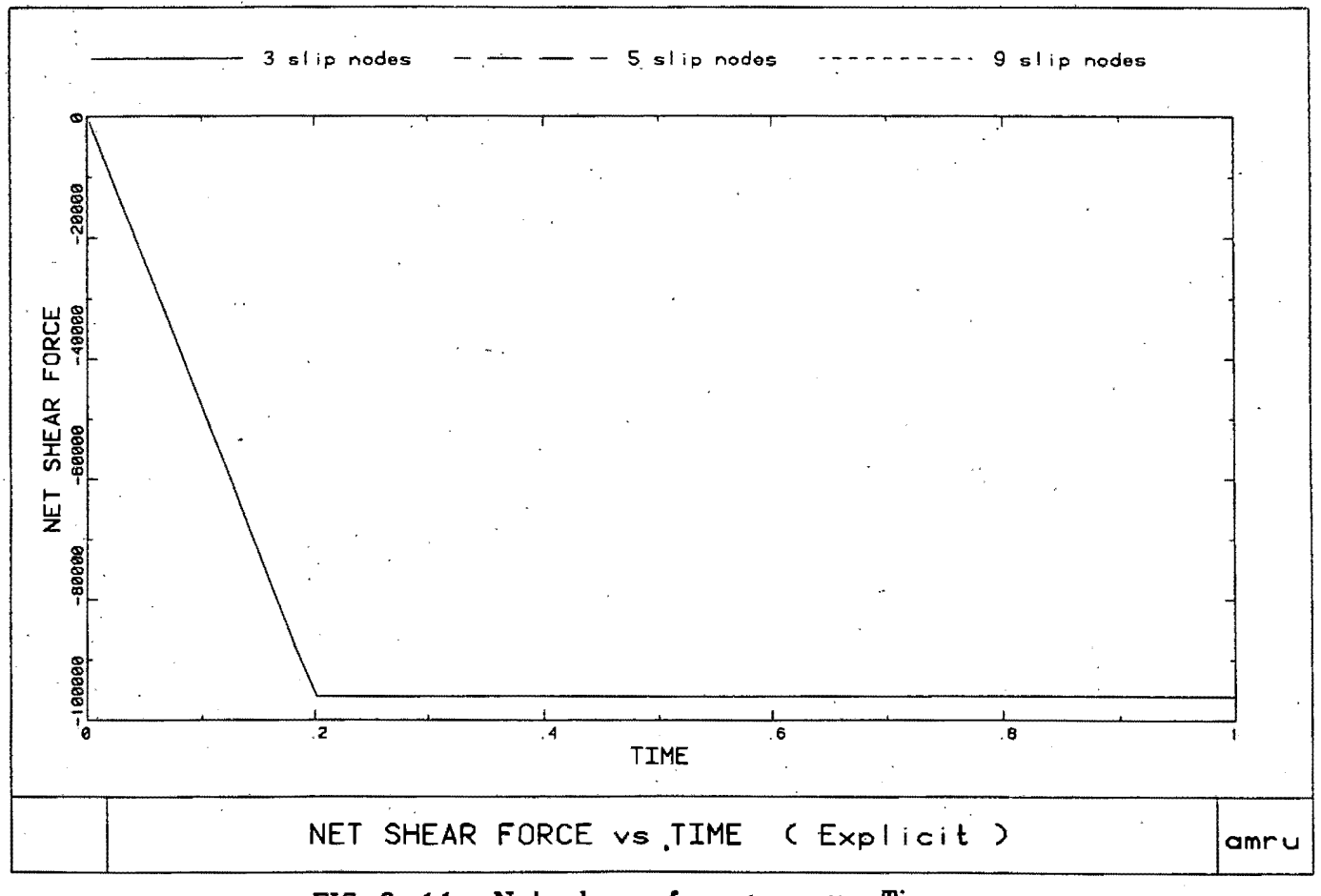

FIG 6–11 Net shear force versus Time.
Explicit Integration.

average normal slip, average shear slip, net normal force and net shear force have been plotted against time for an explicit integration scheme and these are shown in Figure 6.8, 6.9, 6.10 and 6.11. The first three curves show a convergence to a stable value. A very significant feature of the graphs is the relation between the average normal force and the average shear slip. As shear slip occurs the joint dilates or opens. This positive opening causes a negative, compressive force in the beam which acts a stabilising influence and limits further shear slip taking place along the joint.

The graph in Figure 6.11 shows the net shear force plotted against time. This is the same as the loading history.

From the results shown, it was decided to use the 5 noded slip line. This mesh configuration gave consistent results within a reasonable time for all the integration schemes.

6.3.2 Beam with two slip lines

By increasing the number of slip lines in the mesh it was possible to model the hanging wall beam observed in deep mines. The mesh shown in Figure 6.12 shows the half beam with two slip lines 0.25 m from each end. Similar results have been obtained which compare with the single slip line. The average normal dislocation, average shear slip, net normal force and net shear force for an implicit Crank-Nicholson integration scheme are shown in Figures 6.13, 6.14, 6.15 and 6.16 respectively.

The net shear and normal force across the slip lines shown in Figure 6.15 and 6.16 display behaviour consistent with standard beam theory and what would be intuitively obvious. The net normal force across each joint is identical. This must be true otherwise horizontal equilibrium would not hold true and the beam

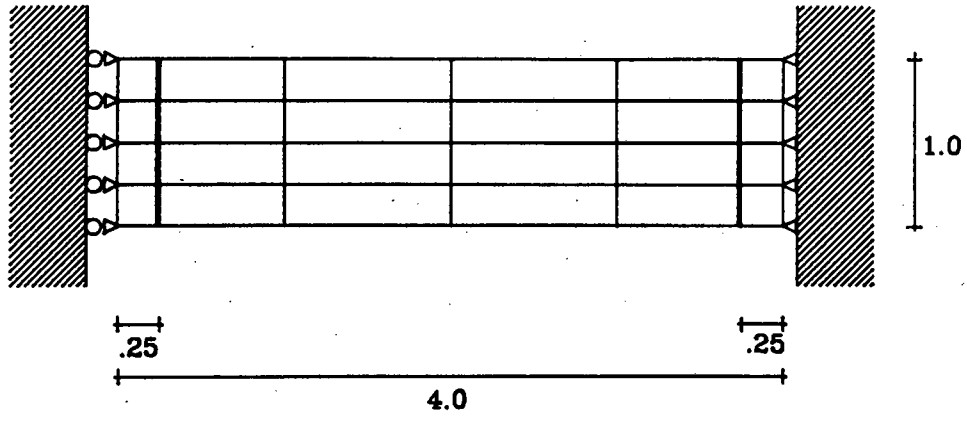

Finite element mesh for hanging wall beam with two slip lines, 5 nodes per slip line.

FIG 6–12

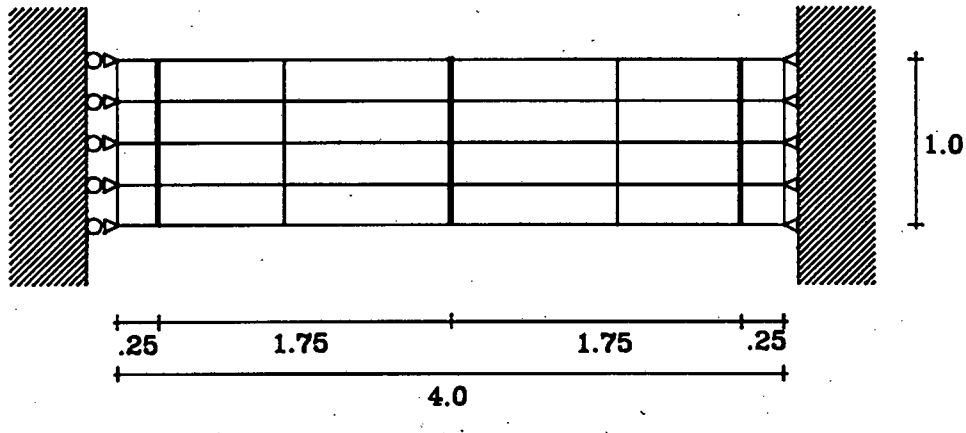

Finite element mesh for hanging wall beam with three slip lines, 5 nodes per slip line.

FIG 6–17

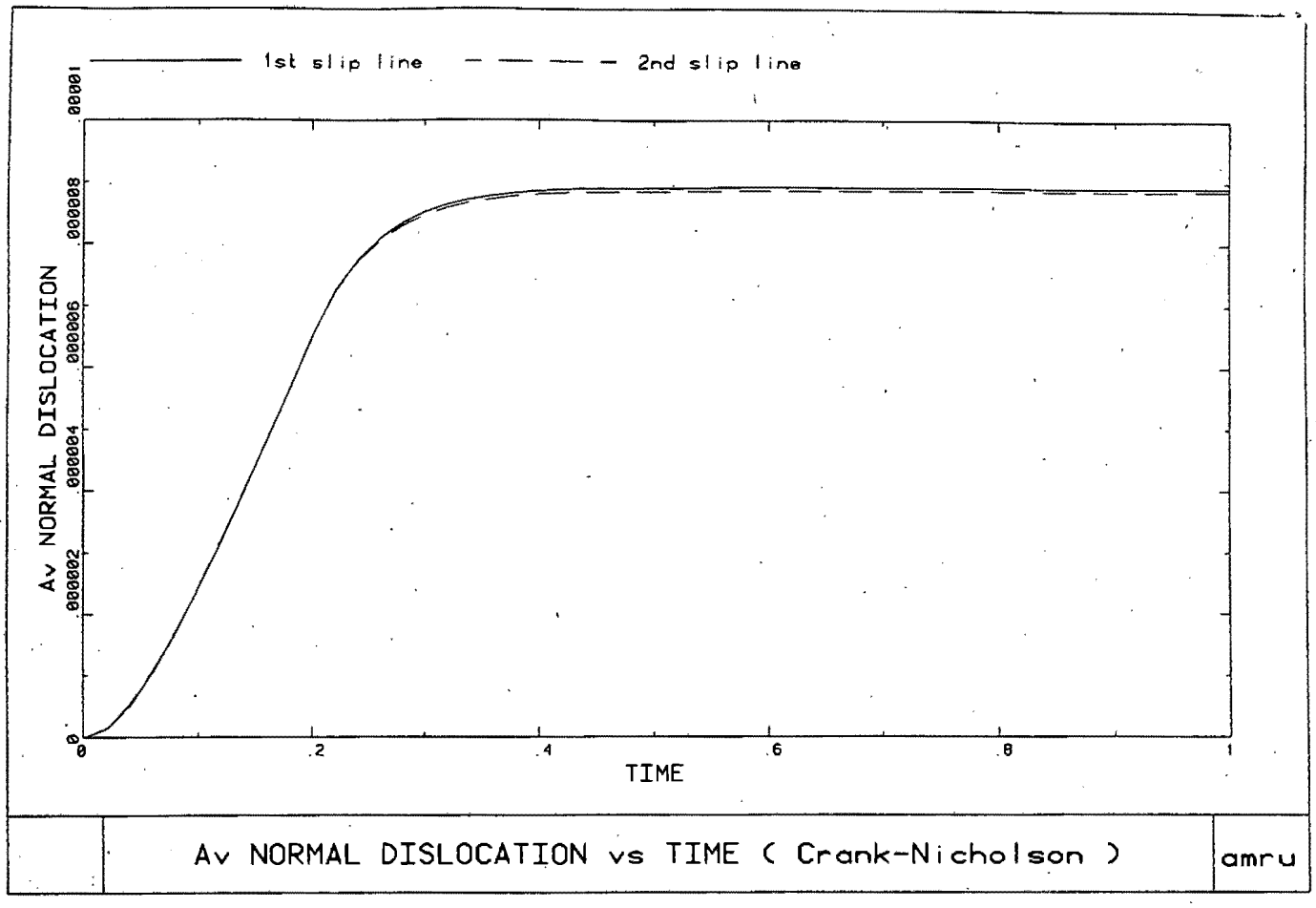

FIG 6–13 Average normal dislocation versus Time.
Crank–Nicholson Integration.

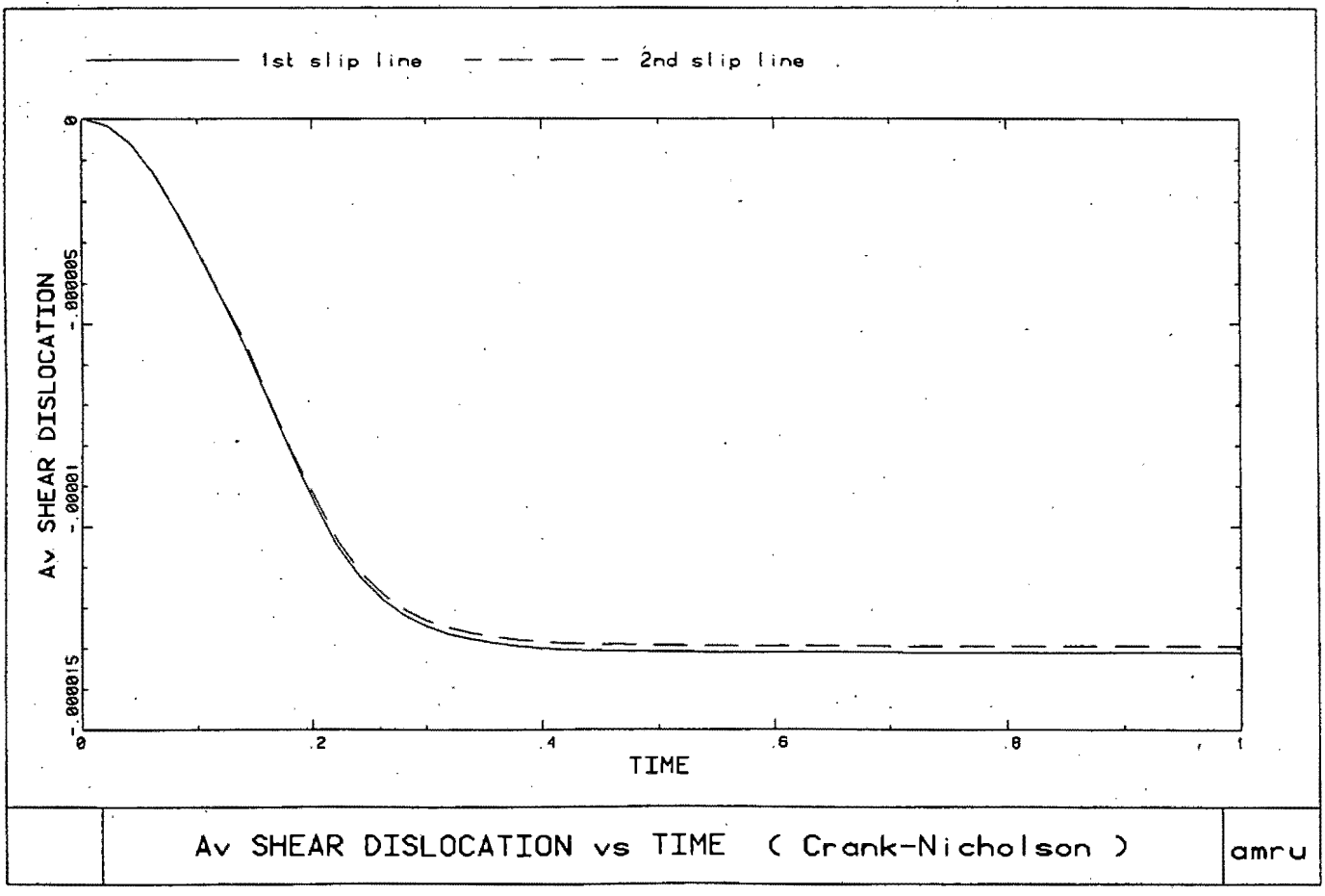

FIG 6–14 Average shear dislocation versus Time.
Crank–Nicholson Integration.

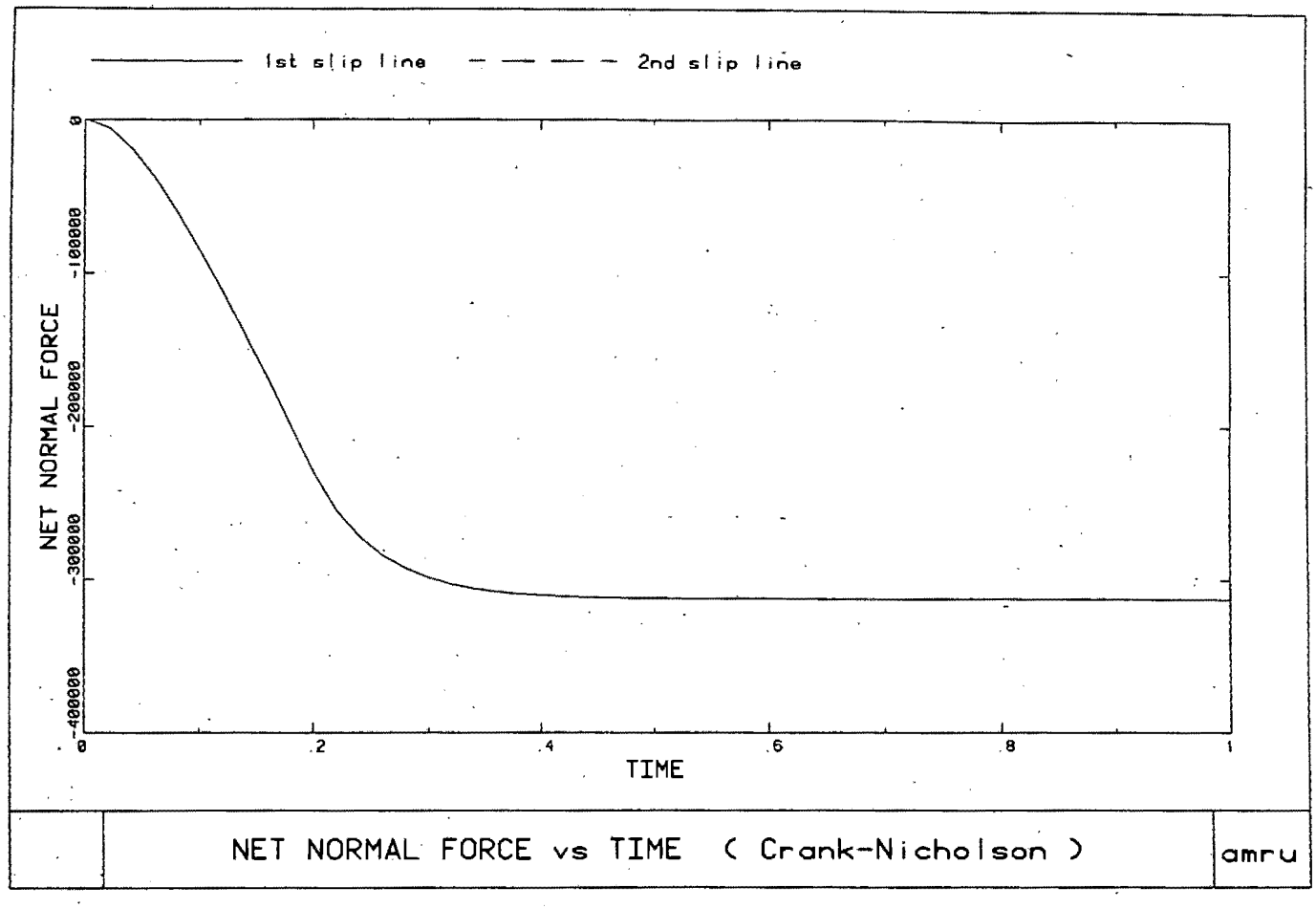

FIG 6-15 Net normal force versus Time.
Crank-Nicholson Integration.

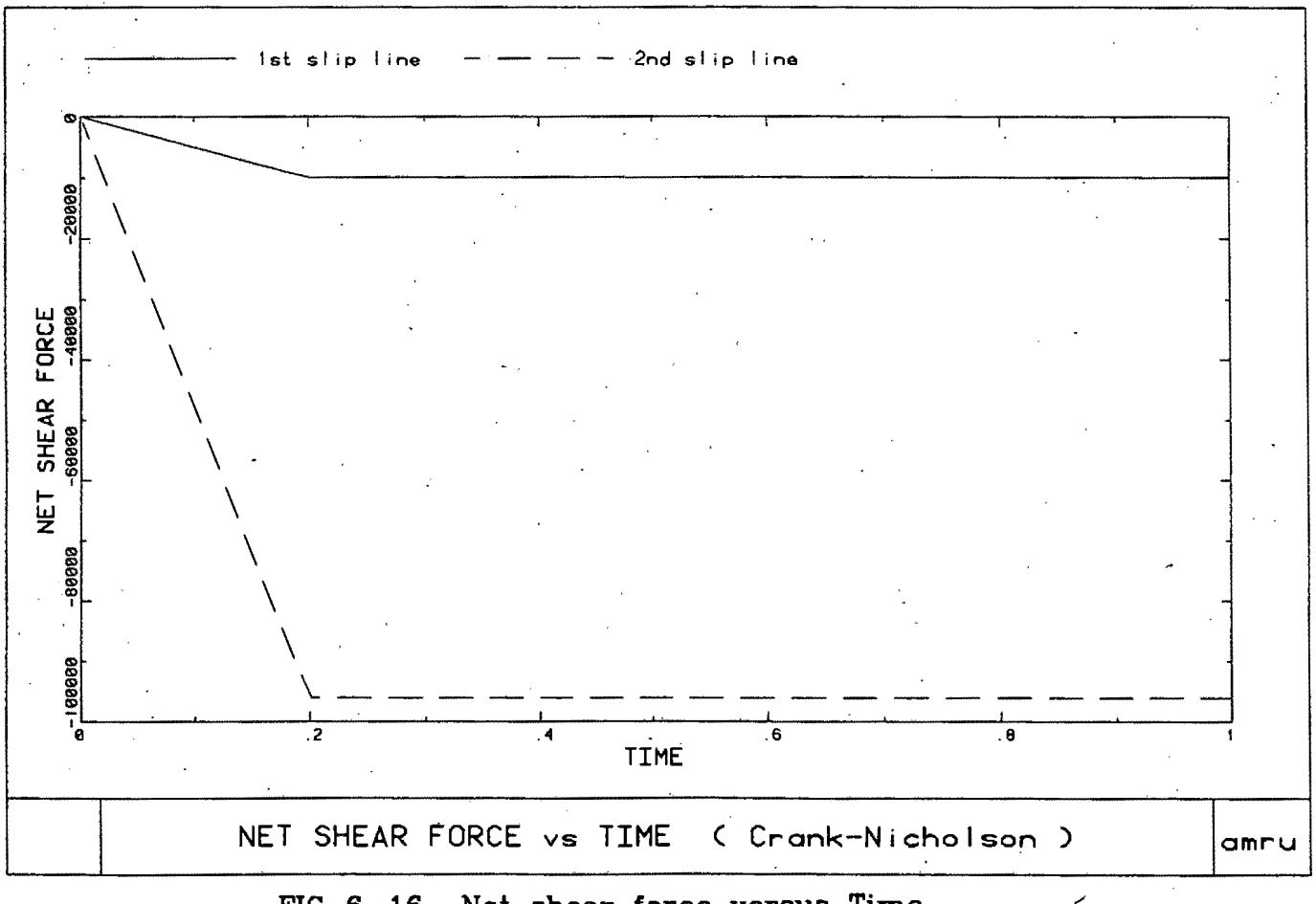

FIG 6-16 Net shear force versus Time.
Crank-Nicholson Integration.

would have horizontal accelerations. The net shear force acting along each joint compares with the shear forces expected on a uniformly loaded beam.

The average normal dislocation across each joint is shown in Figure 6.13. These are similar because of the same normal force across each joint.

However, the same cannot be said of the similarity in the average shear slip in each joint as shown in Figure 6.14. This similarity is believed to occur because of the combined influence of the increase in normal stress on the compression side of the beam due to bending and the normal dilation of each joint. Although the shear force at the fixed end is much larger than that in the centre, the bending moment at the fixed end is double the bending moment at the centre of the beam. The bending combined with dilation increases the normal force which "overcomes" the shear force and limits the shear slip by jamming the beam horizontally. At the left hand of the half span the normal force induced by bending and the shear force are of much smaller magnitude but the mechanism of slipping and jamming remains the same.

6.3.3 Beam with three slip lines

The finite element mesh shown in Figure 6.17 has an additional slip line in the centre of the half span. The results of the same beam with three vertical joints are shown in Figure 6.18, 6.19, 6.20 and 6.21. These results compare very closely with the results of the previous beam. One important point of major interest is the magnitude of shear slip occurring in the slip lines in each beam. Each slip line in the beam with three joints, slips less than the joints in the beam with two joints. This happens because the total dilation occurring in the beam gets progressively larger as the number of slip lines increases.

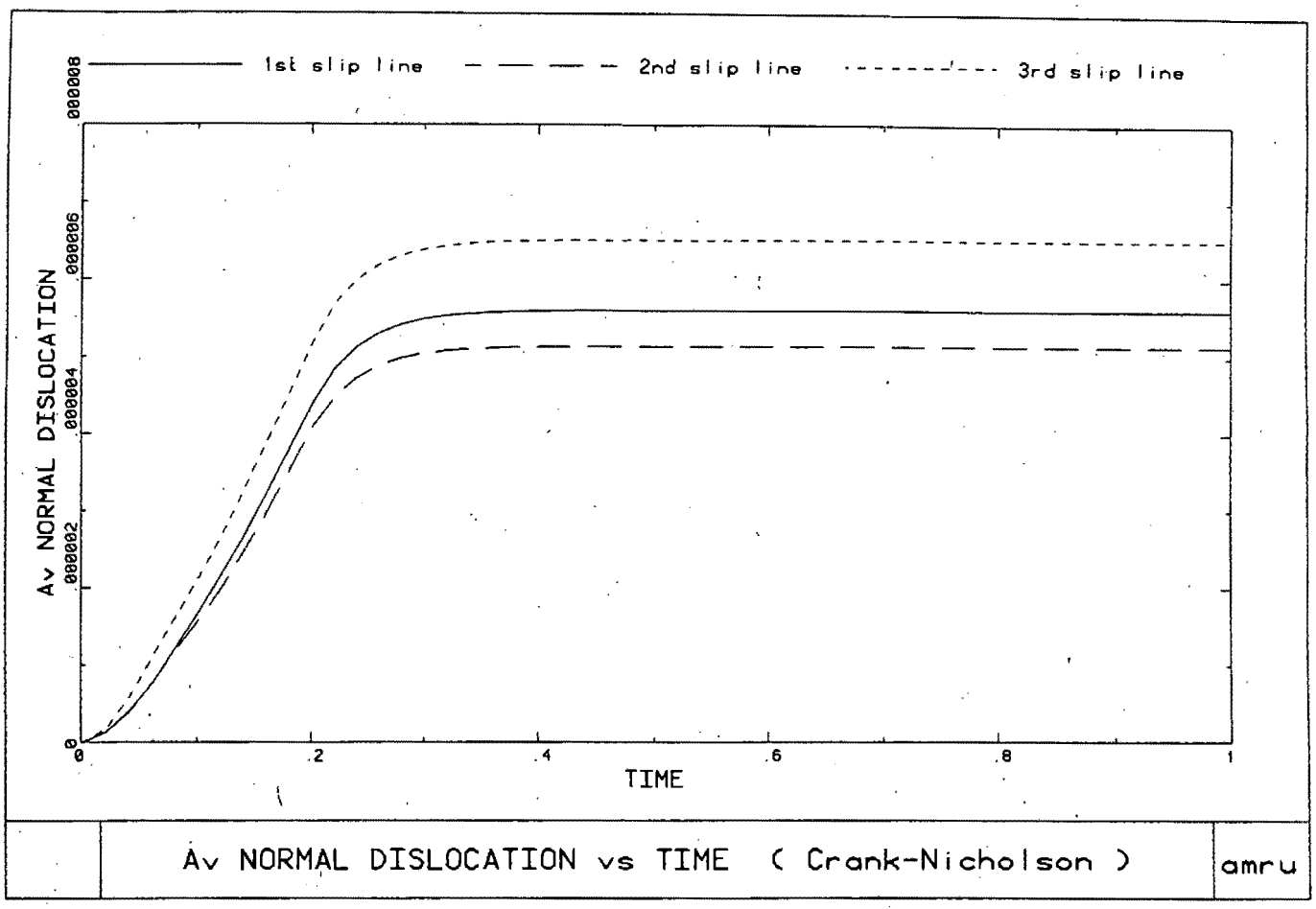

FIG 6-18 Average normal dislocation versus Time.
Crank-Nicholson Integration.

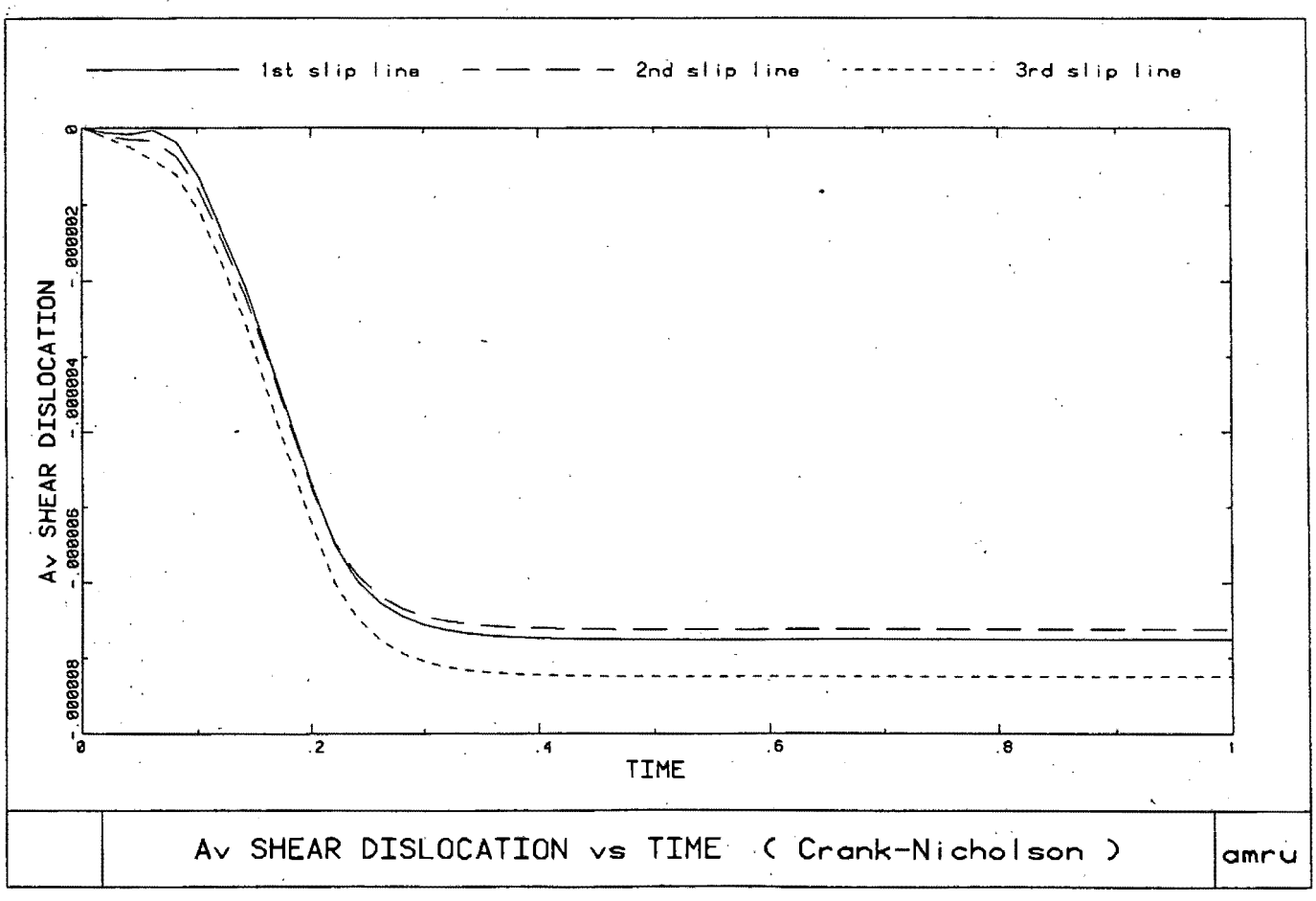

FIG 6-19 Average shear dislocation versus Time.
Crank-Nicholson Integration.

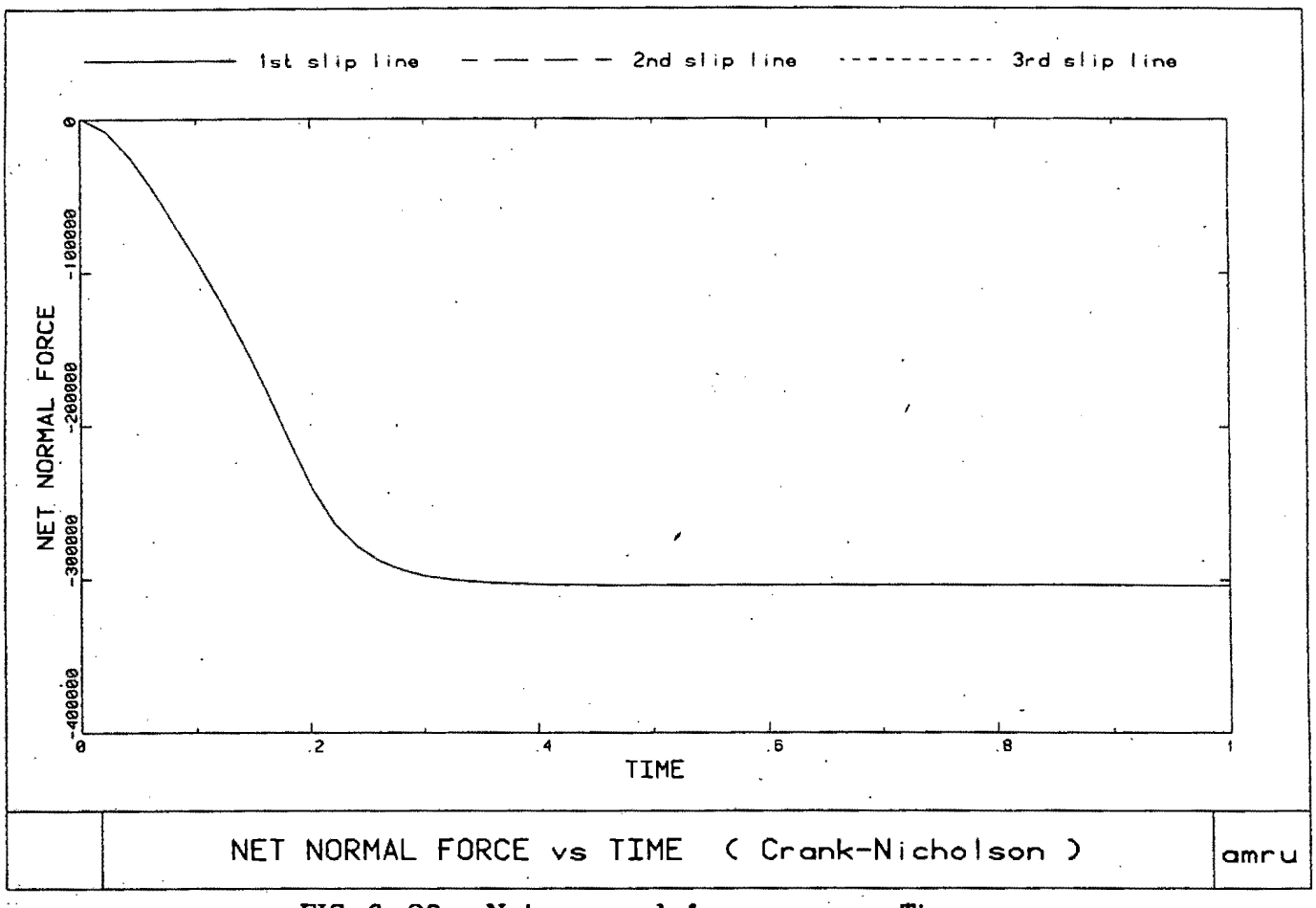

FIG 6-20 Net normal force versus Time.
Crank-Nicholson Integration.

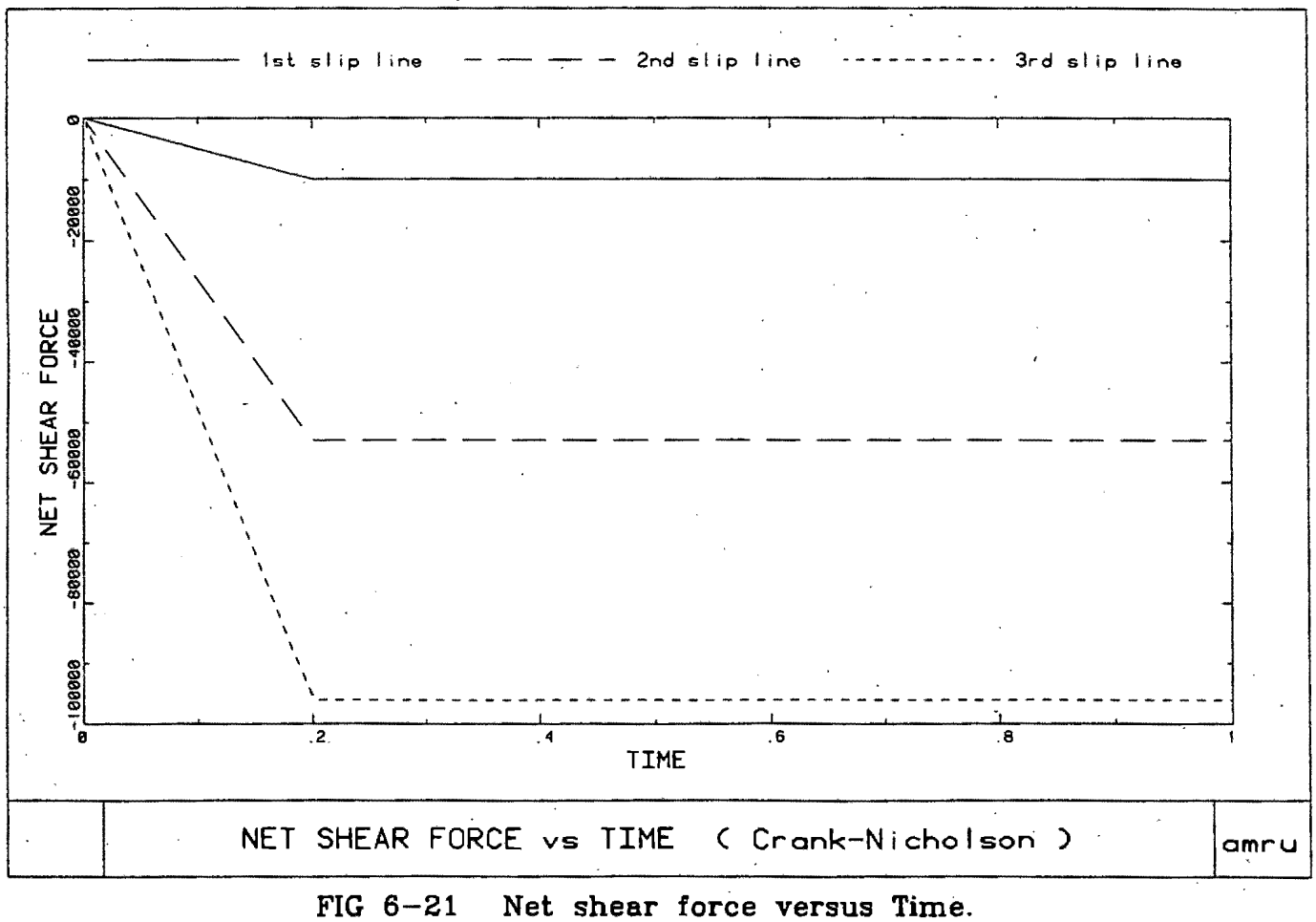

FIG 6-21 Net shear force versus Time.
Crank-Nicholson Integration.

The full net compressive force is reached for a smaller amount of shear slip at each joint and consequently "jamming" of the beam occurs for a smaller shear slip.

6.4 STOPE WITH AN INCLINED DISLOCATION AHEAD OF THE FACE

This example is an idealisation of the fracture pattern proposed by Brummer [37]. The overall dimensions of this example are given in Figure 6.22 and the finite element model is given in Figure 6.23. Infinite elements are used in this model and these are denoted by the dashed lines. The same plots of average normal dislocation, average shear slip, net normal force and net shear force are shown in Figures 6.24, 6.25, 6.26 and 6.27 respectively.

Stability of the normal and shear dislocations takes place rapidly after the full load has been applied. Both the net normal and shear forces stabilize very quickly after full load application has taken place. An interesting feature of the change in the shear force with time is the slight reduction in shear force after the load has been applied. It is thought that any relaxation that takes place as the load is applied is masked by the increasing load. As soon as the load reaches a constant value, the full relaxation, which is shown in Figure 6.27, can take place.

6.5 CONCLUSIONS

A number of different numerical examples are presented in this chapter. They range from the simple plane strain "block" problem to an inclined joint in an infinite rock mass. It is clear from these examples that the internal variable formulation gives good qualitative results for a broad range of mining problems where joints are encountered.

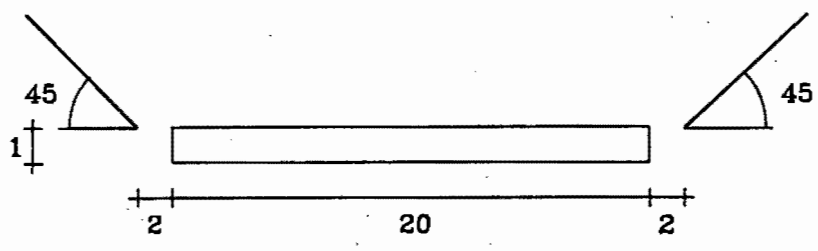

Idealised stope showing slip line and dimensions.

FIG 6-22

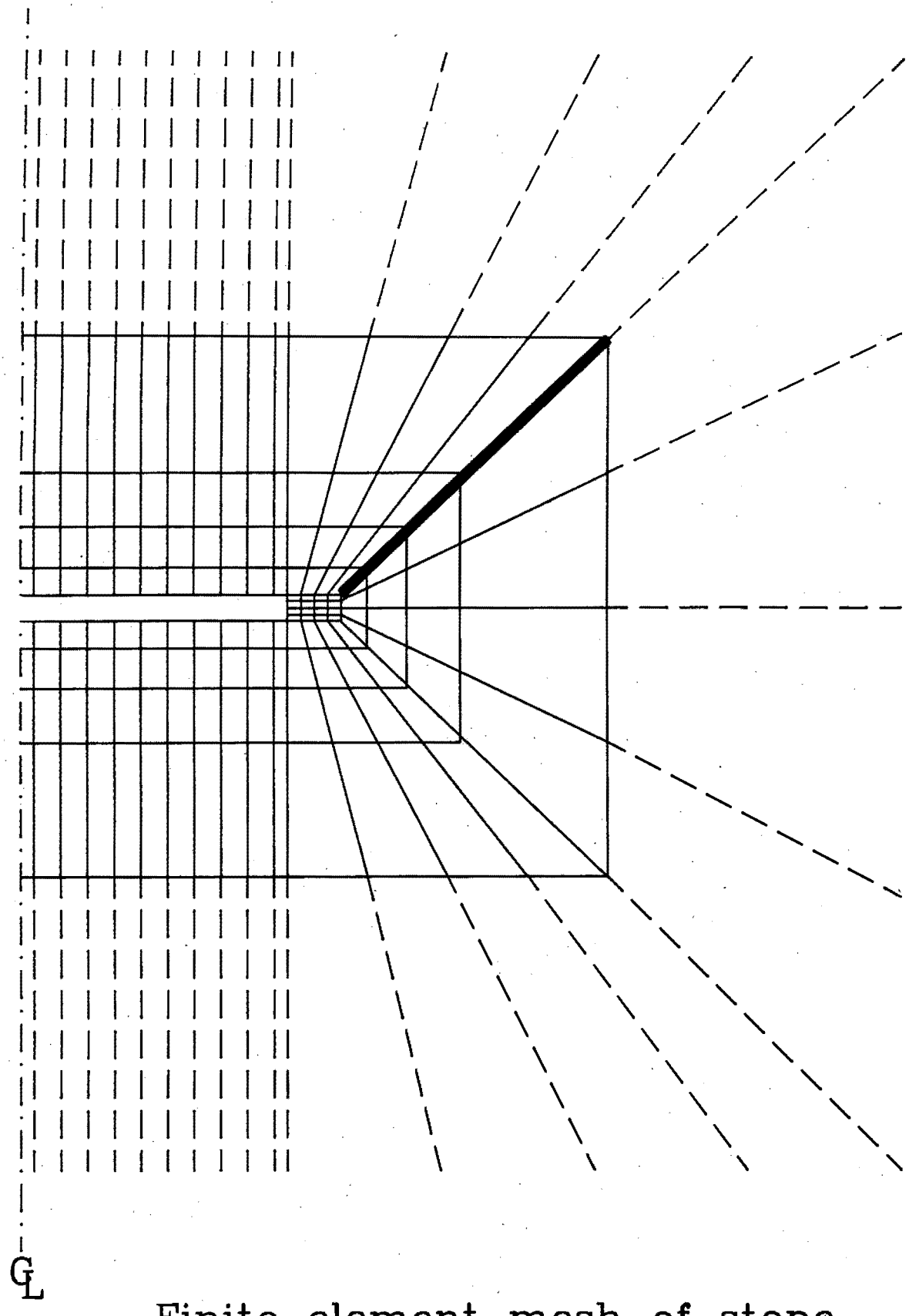

Finite element mesh of stope with 45 degree slip line.

FIG 6–23

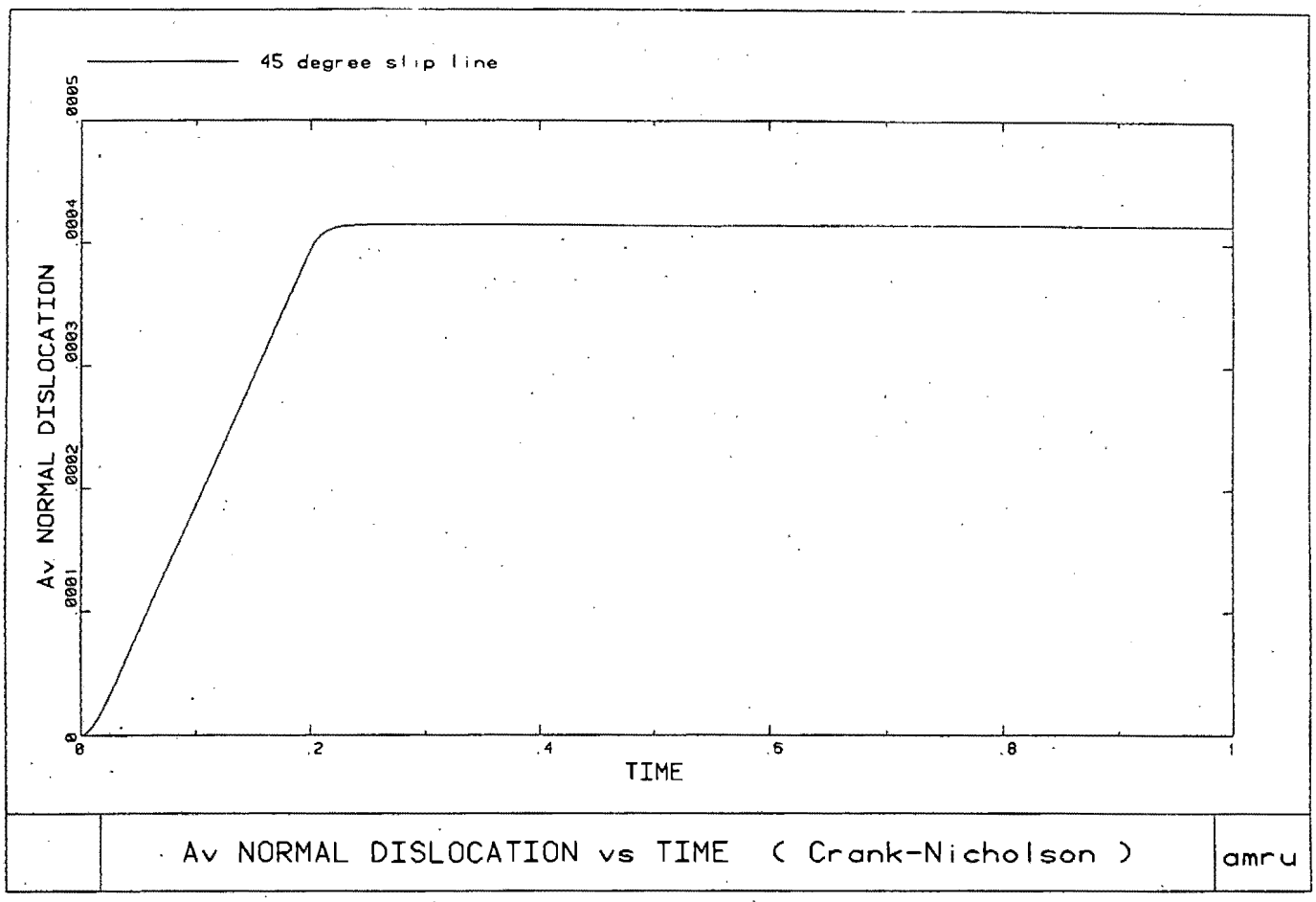

FIG 6-24 Average normal dislocation versus Time. Crank-Nicholson Integration.

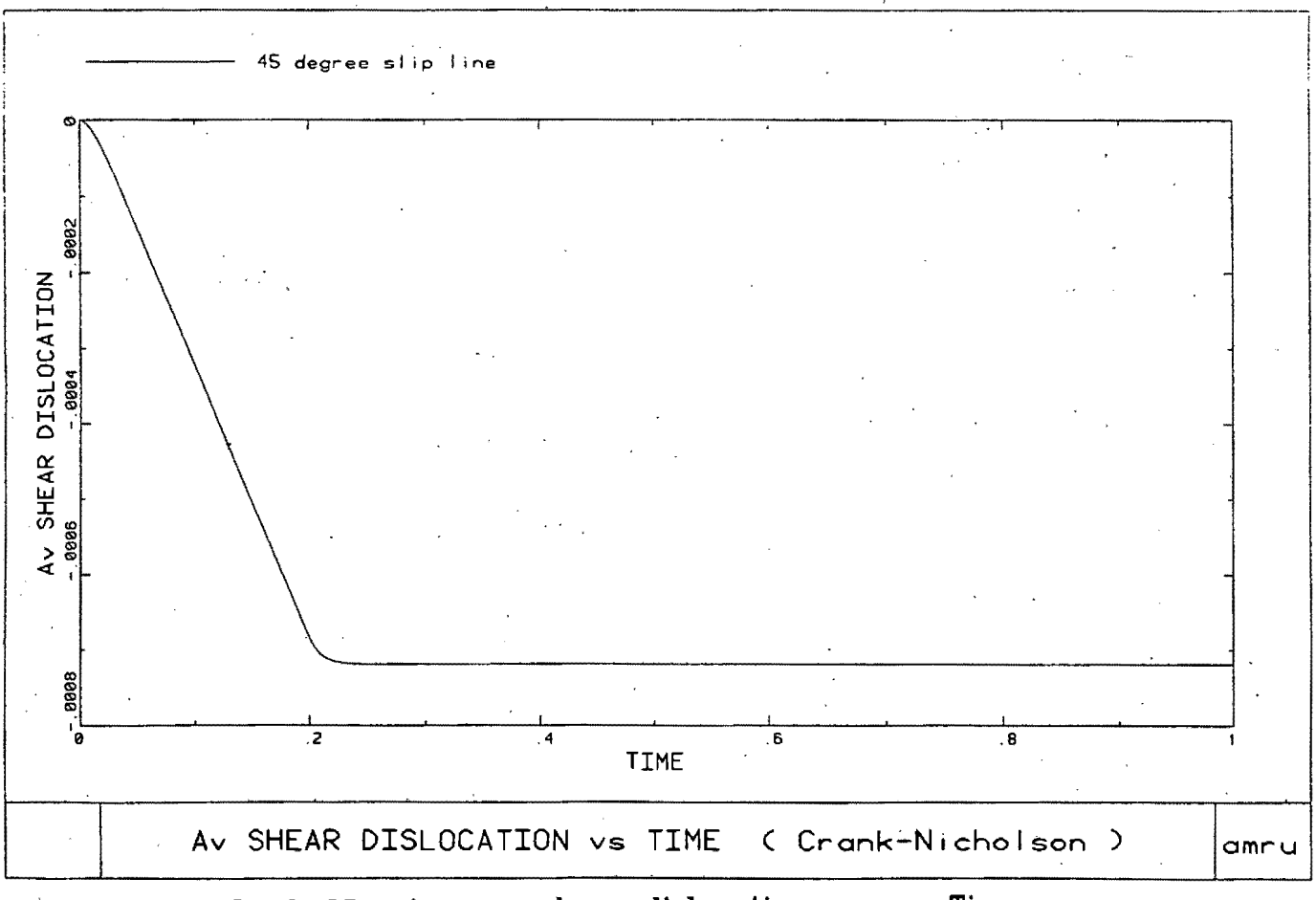

FIG 6-25 Average shear dislocation versus Time. Crank-Nicholson Integration.

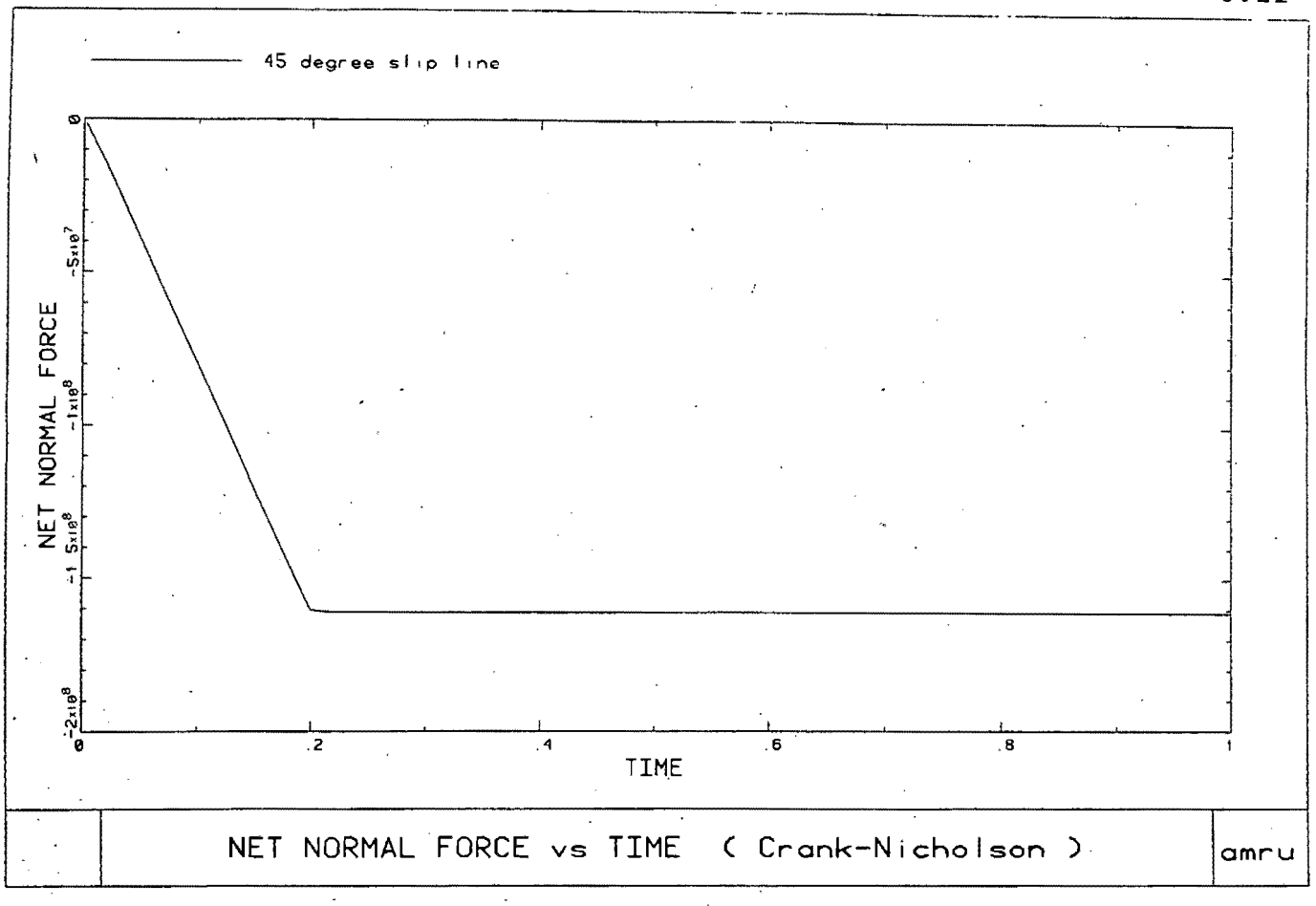

FIG 6–26 Net normal force versus Time. Crank–Nicholson Integration.

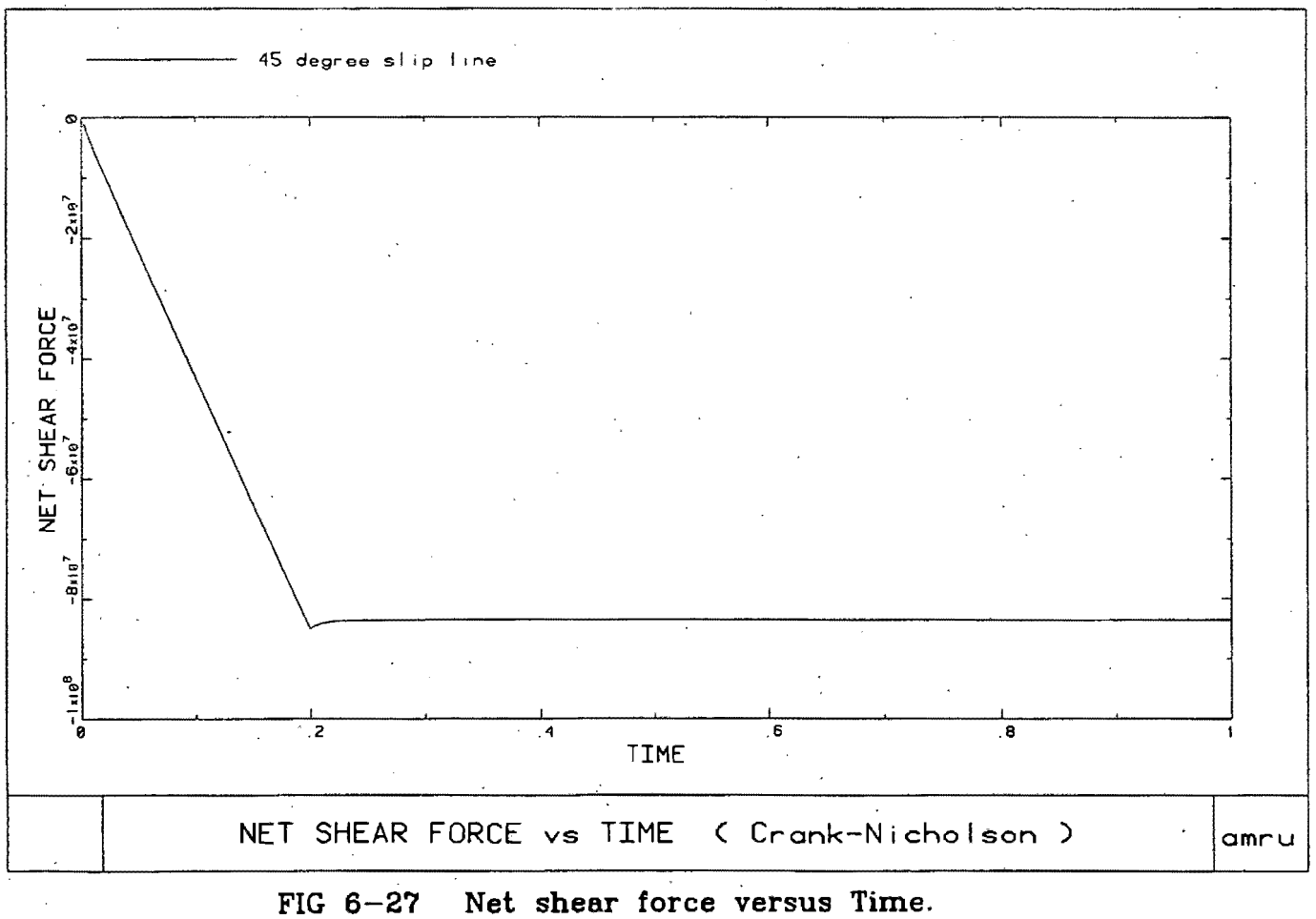

FIG 6–27 Net shear force versus Time. Crank–Nicholson Integration.

CHAPTER 7

CONCLUSIONS

A method for analysing the time dependent behaviour of jointed rock masses has been presented. An internal variable method has been used to calculate the internal nodal forces and dislocations. The time dependent effects were modelled using a viscoplastic constitutive law with a hyperbolic yield function. The method was computerised and solutions to various problems were carried out using the finite element program, NOSTRUM.

The internal variable method presented in this study does not suffer from the numerical difficulties found in specially designed joint elements. The hyperbolic yield function can be made to approximate the Mohr-Coulomb yield function which is commonly used in rock mechanics problems. The hyperbolic yield function has the advantage of being continuously differentiable and this eliminates the singularity of the vertex point in the Mohr-Coulomb yield function. Both explicit and implicit integration schemes were successfully implemented. It was shown that the Crank-Nicholson integration scheme gave results which were both reliable and closely approximated the analytical results.

Various mining problems were presented and analysed. The hangingwall beam problems with one or more slip lines show very definite trends in behaviour. The relationship between shear and normal dislocation is very clear and pronounced. As the beam slips vertically dilation occurs and jams the beam in, thereby stabilizing it. This, in turn, causes a compressive force to be generated in the beam. An increase in the number of slip lines in the beam causes smaller amounts of shear displacement. This is because of an increase in the amount of total dilation across a number of slip lines for a given length of beam. In all cases the net normal force in the beam is the same. This is expected because the "driving force" behind any movement is the self-weight of the beam. The method was also shown to work for a much larger problem where the results which were obtained were explained satisfactorily.

The results presented give an insight into the essential features of some mining problems, rather than precise numerical answers to particular cases.

It was expected that the implicit integration schemes would allow a much longer time step length to be used. It was found that only doubling of the time step length was possible for convergence to be obtained within the chosen number of iterations. A more detailed consideration of the convergence scheme might enable one to use longer time steps.

BIBLIOGRAPHY

1. BELYTSCHKO, T., PLESHA, M. & DOWDING, C.H.; A Computer Method for Stability Analysis of Caverns in Jointed Rock, Int. J. Num. Anal. Meth. Geomech., Vol. 8, 1984, pp. 473-492.

2. PATTON, F.D.; Multiple Modes of Shear Failure in Rock, Proceedings of 1st Congress ISRM, Lisbon, Vol. 1, 1966, pp.509-513.

3. KRAHN, J. & MORGENSTERN, N.R.; The Ultimate Frictional Resistance of Rock Discontinuities, Int. J. Rock. Mech. Min. Sci. & Geomech. Abstr., Vol. 16, 1979, pp. 127-133.

4. REEVES, M J.; Rock Surface Roughness and Frictional Strength, Int. J. Rock. Mech. Min. Sci. & Geomech. Abstr., Vol. 22, No. 6, 1985, pp. 429-442.

5. DIGHT, P.M. & CHIU, H.K.; Prediction of Shear Behaviour of Joints Using Profiles, Int. J. Rock. Mech. Min. Sci. & Geomech. Abstr., Vol. 18, 1981, pp. 369-386.

6. BANDIS, S., LUMSDEN, A.C. & BARTON, N.R.; Experimental Studies of Scale Effects on the Shear Behaviour of Rock Joints, Int. J. Rock Mech. Min. Sci. & Geomech. Abstr., Vol. 18, 1981, pp. 1-21.

7. ROBERDS, W.J. & EINSTEIN, H.H.; Comprehensive Model for Rock Discontinuities, Journal of the Geotechnical Engineering Division, ASCE, Vol. 104, No. GT5, May 1978, pp. 553-569.

8. SOFIANOS, A.I.; Stability of Rock Wedges in Tunnel Roofs, Int. J. Rock. Mech. Min. Sci. & Geomech. Abstr., Vol. 23, No. 2, 1986, pp. 119-130.

9. GOODMAN, R.E. & DUBOIS, J.; Duplication of Dilatancy in Analysis of Jointed Rocks, Journal of Soil Mechanics and Foundation Division, ASCE, Vol. 98, No. SM4, Proc. Paper, April 1972, pp. 399-422.

10. HEUZE, F.E. & BARBOUR, T.G.; New Models for Rock Joints and Interfaces, Journal of the Geotechnical Engineering Division, ASCE, Vol. 108, No. GT5, May 1982, pp. 757-776.

11. GOODMAN, R.E., TAYLOR, R.L. & BREKKE, T.L.; A Model for the Mechanics of Jointed Rock, Journal of the Soil Mechanics and Foundation Division, ASCE, Vol. 94, No. SM3, Proc. Paper 5937, May 1968, pp. 637-659.

12. GOODMAN, R.E.; Deformability of Joints, ASTM, STP 477, 1970, p. 174.

13. LADANYI, B. & ARCHAMBAULT, G.; Simulation of Shear Behaviour of Jointed Rock Mass, Proceedings 11th Symposium on Rock Mechanics, American Institute of Mining, Metalurgical and Petroleum Engineers, 1970, pp. 83-104.

14. GHABOUSSI, J, WILSON, E.L. & ISENBERG, J.; Finite Element for Rock Joints and Interfaces, Journal of Soil Mechanics and Foundation Division, ASCE, Vol. 99, No. SM10, Oct. 1973, pp. 833-848.

15. BARTON, N.R.; The Shear Strength of Rock and Rock Joints, Int. J. Rock Mech., Min. Sci. & Geomech. Abstr., Vol. 13, 1976, pp. 255-279.

16. GOODMAN, R.E. & ST. JOHN, C.; Finite Element Analysis for Discontinuous Rocks, Chapter 4, Numerical Methods in Geotechnical Engineering, McGraw-Hill, New York, 1976.

17. PANDE, G.N.; Numerical Modelling of Rocks, Possibilities and Problems, 3rd International Conference on Numerical Methods in Geomechanics, Aachen, 2-6 April 1979, pp. 1341-1356.

18. HEUZE, F.E.; Dilatant effects of rock joints. Proceedings of 4th Congress, ISRM, Montreaux, Switzerland, Vol. 1, Sept. 1979, pp. 169-175.

20. MARTIN, J.B.; An Internal Variable Approach to the Formulation of Finite Element Problems in Plasticity, Physical non-linearities in Structural Analysis, eds. J. Hult & J. LeMaitre. Springer - Verlag, 1981, pp. 165-176.

21. MARTIN, J.B.; Virtual Work, Material Inequalities and Variational Principles in Structural Mechanics, Survey Lecture delivered to Annual Conference of the S A Mathematical Soc., Port Elizabeth, October 1981.

22. NAYLOR, D.J., PANDE, G.N., SIMPSON, B. & TABB, R.; Finite Elements in Geotechnical Engineering, Chapter 5, Pineridge Press, Swansea, U.K. 1976.

23. ZIENKIEWICZ, O.C. & PANDE, G.N.; Some Useful Forms of Isotropic Yield Surfaces for Soil and Rock Mechanics, Chapter 5, Finite Elements in Geomechanics (Ed. Gudehus G) Pineridge Press, Swansea, 1977.

24. EVE, R.A., REDDY, B.D. & ROCKAFELLAR, R.T.; An Internal Variable Theory of Elastoplasticity Based on the Maximum Plastic Work Inequality, AMRU Report 110, University of Cape Town, April 1988.

25. MARTIN, J.B.; Plasticity: Fundamental and General Results, MIT Press, Massachusetts, 1975, pp. 100-110.

26. GERADIN, M., HOGGE, M. & IDELSOHN, S.; Implicit Finite Element Methods, Computational Methods for Transient Analysis, Chap. 9, pp.417-471, 1983.

27. OWEN, D.R.J. & HINTON, E.; Finite Element In Plasticity, Theory & Practice, Trowbridge, Pineridge Press, 1980.

28. KANCHI, M.B., ZIENKIEWICZ, O.C. & OWEN, D.R.J.; The Visco-Plastic Approach to Problems of Plasticity and Creep Involving Geometric non-Linear Effects, Int. J. Num. Meth. Eng., Vol. 12, pp. 169-181, 1978.

29. ZIENKIEWICZ, O.C.; The Finite Element Method in Engineering Science, 3rd edition, McGraw-Hill, London, 1977.

30. ZIENKIEWICZ, O.C. & CORMEAU, I.C.; Visco-Plasticity - Plasticity and Creep in Elastic Solids - A Unified Numerical Solution Approach, Int. J. Num. Meth. Eng., Vol. 8, 1974, pp. 821-845.

31. LEVY, A. & PIFKO, A.B.; On Computational Strategies for Problems Involving Plasticity and Creep, Int. J. Num. Meth. Eng., Vol. 17, 1981, pp. 747-771.

32. FRITZ, P.; Numerical Solution of Rheological Problems in Rock, International Symposium on Numerical Models in Geomechanics, Zurich, 13-17 September, 1982, pp. 793-803.

33. CORMEAU, I.; Numerical Stability in Quasi-Static Elasto/ Visco-Plasticity, Int. J. Num. Meth. Eng., Vol. 9, 1975, pp. 109-127.

34. LAMA, R.D. & VUTUKURI, V.S.; Handbook on Mechanical Properties of Rock, Vol. III, Chapter 9, Aedermansdorf, Switzerland, Trans. Tech. SA. 1978.

35. STAGG, K.G. & ZIENKIEWICZ, O.C.; Rock Mechanics in Engineering Practice, John Wiley & Sons, London, 1969.

36. JAEGER, J.C. & COOK, N.G.W.; Fundamentals of Rock Mechanics, Methuen & Co., London, 1969.

37. BRUMMER, R.K.; A Simplified Modelling Strategy for describing Rock Mass Behaviour around Stope Faces in Deep Hard-Rock Gold Mines, 26th U.S. Symposium on Rock Mechanics, Rapid City, SD, 26-28 June 1985, pp. 113-120.

38. BRUMMER, R.K.; Modelling the Nonlinear Behaviour of Fractured Seams in Deep Gold Mines, 20th Int. Symposium on Application of Computers and Mathematics in Mineral Industries, Johannesburg, Vol. 1, 1987, pp. 21-32.